

An overview of η and η' decays at BESIII*

Shuang-shi Fang^{1,2,4} Andrzej Kupsc³ Dai-hui Wei⁴

¹ Institute of High Energy Physics, Chinese Academy of Science, 100049 Beijing, People's Republic of China

² University of Chinese Academy of Sciences, 100049 Beijing, People's Republic of China

³ Uppsala University, Box 516, SE-75120 Uppsala, Sweden

⁴ Guangxi Normal University, Guilin 541004, People's Republic of China

Abstract:

The world's largest sample of 1.31 billion J/ψ events accumulated at the BESIII detector, provides a unique opportunity to investigate η and η' physics via two body J/ψ radiative or hadronic decays. For many η' decay channels the low background data samples are up to three orders of magnitude larger than collected in any previous experiment. Here we review the most significant results on η and η' obtained at BESIII so far. The analyses range from detailed studies of the common decays dynamics, observations of new radiative and Dalitz decays, and search for rare/forbidden decays with sensitivity up to $\mathcal{B} \sim 10^{-5}$. Finally, prospects of the forthcoming runs at J/ψ peak for the η and η' physics are discussed.

Key words: η/η' decays, the BESIII detector

PACS: 13.20.-v, 14.40.Be

1 Introduction

More than half a century after η [1] and η' [2, 3] discoveries, the mesons still attract attention of both theory and experiment. As the neutral members of the ground state pseudoscalar nonet, they play an important role in understanding low energy Quantum Chromodynamics (QCD). The main properties of η and η' mesons are firmly established and their main decay modes are fairly well known. Decays of the η/η' probe a wide variety of physics issues *e.g.* π^0 - η mixing, light quark masses and pion-pion scattering. In particular the η' meson, much heavier than the Goldstone bosons of broken chiral symmetry, plays a special role as predominantly the singlet state arising from the strong axial $U(1)$ anomaly. In addition the decays of both mesons are used to search for processes beyond any considered extension of the Standard Model (SM) and to test fundamental discrete symmetries.

The main decays of the η/η' meson are hadronic and radiative processes. Alternatively one can divide the decays into two following classes. The first class consists of hadronic decays into three pseudoscalar mesons, such as $\eta' \rightarrow \eta\pi\pi$. Those processes are already included

in the lowest order, $\mathcal{O}(p^2)$, of chiral perturbation theory (ChPT) [4]. The second class includes anomalous processes involving odd number of pseudoscalar mesons, such as $\eta' \rightarrow \rho^0\gamma$ and $\eta' \rightarrow \pi^+\pi^-\pi^+\pi^-$. They are driven by the Wess-Zumino-Witten (WZW) term [5, 6] which enters at $\mathcal{O}(p^4)$ order [7]. Dynamics of η decays remains a subject of extensive studies aiming at precision tests of ChPT in $SU_L(3) \times SU_R(3)$ sector (*i.e.* involving s quark). Model-dependent approaches for describing low energy meson interactions, such as Vector Meson Dominance (VMD) [8, 9], and the large number of colors, N_C , extensions of ChPT [10] together with dispersive methods could be extensively tested in η' decays.

Table 1. The available η/η' decays calculated with the 1.31×10^9 J/ψ events at BESIII.

| Decay Mode | $\mathcal{B} (\times 10^{-4})$ [17] | η/η' events |
|----------------------------------|-------------------------------------|---------------------|
| $J/\psi \rightarrow \gamma\eta'$ | 51.5 ± 1.6 | 6.7×10^6 |
| $J/\psi \rightarrow \gamma\eta$ | 11.04 ± 0.34 | 1.4×10^6 |
| $J/\psi \rightarrow \phi\eta'$ | 7.5 ± 0.8 | 9.8×10^5 |
| $J/\psi \rightarrow \phi\eta$ | 4.5 ± 0.5 | 5.9×10^5 |

The BESIII detector [16], operating at the Beijing

Received X X X

* This article is supported in part by National Natural Science Foundation of China (NSFC) under Contract No. 11565006, 11675184, 11735014

1) E-mail: fangss@ihep.ac.cn

2) E-mail: Andrzej.Kupsc@physics.uu.se

3) E-mail: weidh@gxnu.edu.cn

©2013 Chinese Physical Society and the Institute of High Energy Physics of the Chinese Academy of Sciences and the Institute of Modern Physics of the Chinese Academy of Sciences and IOP Publishing Ltd

Table 2. Some of the BESIII results on η' branching fractions, \mathcal{B} , based on the sample of 1.31×10^9 J/ψ events. Extracted yields with statistical errors, detection efficiency and branching fractions for the studied η' decay modes, where the first error is statistical, the second systematic, and the third from model dependence. The last column gives the status before BESIII experiment.

| Decay Mode | Yield | ε (%) | \mathcal{B} ($\times 10^{-4}$) | Ref. | Comment |
|--|-----------------|-------------------|------------------------------------|------|-----------------------|
| $\eta' \rightarrow \pi^+\pi^-\pi^0$ | 6067 ± 91 | 25.3 | $35.91 \pm 0.54 \pm 1.74$ | [11] | previously 20 events |
| $(\pi^+\pi^-\pi^0)_S$ | 6580 ± 130 | 26.2 | $37.63 \pm 0.77 \pm 2.22 \pm 4.48$ | [11] | first measurement |
| $\rho^\pm\pi^\mp$ | 1231 ± 98 | 24.8 | $7.44 \pm 0.60 \pm 1.26 \pm 1.84$ | [11] | first measurement |
| $\eta' \rightarrow \pi^0\pi^0\pi^0$ | 2015 ± 47 | 8.8 | $35.22 \pm 0.82 \pm 2.60$ | [11] | previously 235 events |
| $\eta' \rightarrow e^+e^-\gamma$ | 864 ± 36 | 24.5 | $4.69 \pm 0.20 \pm 0.23$ | [12] | first measurement |
| $\eta' \rightarrow e^+e^-\omega$ | 66 ± 11 | 5.45 | $1.97 \pm 0.34 \pm 0.17$ | [13] | first measurement |
| $\eta' \rightarrow \gamma\omega$ | 33187 ± 351 | 21.9 | $255.00 \pm 3.00 \pm 16.00$ | [13] | |
| $\eta' \rightarrow \gamma\gamma\pi^0$ | 655 ± 68 | 15.9 | $6.16 \pm 0.64 \pm 0.67$ | [14] | first measurement |
| $\eta' \rightarrow \pi^+\pi^-\pi^+\pi^-$ | 199 ± 16 | 34.5 | $0.853 \pm 0.069 \pm 0.069$ | [15] | first measurement |
| $\eta' \rightarrow \pi^+\pi^-\pi^0\pi^0$ | 84 ± 16 | 7.0 | $1.82 \pm 0.35 \pm 0.18$ | [15] | first measurement |

Electron Positron Collider (BEPCII), is a general purpose facility designed for τ -charm physics studies in e^+e^- annihilation with high precision. Since its commissioning in 2008, a series of important results have been achieved, including charmonium decays, light hadron spectroscopy and charm meson decay, with the world's largest data samples in the τ -charm region. Due to high production rate of light mesons in the charmonium, *e.g.*, J/ψ , decays, the BESIII experiment also offers a unique possibility to investigate the light meson decays. Radiative decays $J/\psi \rightarrow \eta\gamma$ and $J/\psi \rightarrow \eta'\gamma$ provide clean and efficient sources of η/η' mesons for the decay studies. The accompanying radiative photon, with energy of 1.5 GeV/ c^2 and 1.4 GeV/ c^2 respectively, is well separated from the decay products. An alternative source of the η (η') is the hadronic two-body process of $J/\psi \rightarrow \phi\eta$ ($J/\psi \rightarrow \phi\eta'$) where ϕ is identified via $\phi \rightarrow K^+K^-$ decay could be used to tag $\eta(\eta')$ decays where not all decay products are reconstructed.

With two runs in 2009 and in 2012 a total data sample of 1.31×10^9 J/ψ events [18, 19] was collected at the BESIII detector, the available η and η' events are summarized in Table. 1 from radiative decays of $J/\psi \rightarrow \gamma\eta$, $\gamma\eta'$, and hadronic decays of $J/\psi \rightarrow \phi\eta$, $\phi\eta'$.

The review presents a recent progress on η/η' decays at the BESIII experiment. Unless specifically mentioned the analyses are based on the full data sample of 1.31×10^9 J/ψ events. However, some earlier analyses use data from 2009 run only with 225.3×10^6 J/ψ events. A summary of some branching fractions measured by BESIII and the collected data samples using full data set is presented in Table 2. For the common three body η and η' processes results on the decay distributions are reported. In addition the upper limits at 90% confidence level (C.L.) for rare and forbidden decay modes are presented. Finally the prospects for the analyses based on

the 10^{10} J/ψ events to be collected at BESIII in the near future are discussed.

2 η/η' hadronic decays

2.1 $\eta \rightarrow \pi^+\pi^-\pi^0$ and $\eta \rightarrow \pi^0\pi^0\pi^0$ [20]

Decays of the η meson into 3π violate isospin symmetry and were first considered to be electromagnetic transitions. However, it turns out the electromagnetic contribution is strongly suppressed [21–24]. Therefore the decays provide a unique opportunity for a precision determination of m_u/m_d quark mass ratio in a strong process [25]. The challenge for the theory is to provide a model independent description of the process based on ChPT, supplemented by general analytic properties of the amplitudes (dispersive methods). This approach keeps the promise to finally resolve long standing discrepancy between the lowest order ChPT prediction for the decay width of $\eta \rightarrow \pi^+\pi^-\pi^0$ of 66 eV [26] and the experimental value of 300 ± 11 eV [17]. This would conclude several years of efforts put by several theory groups to understand the problem, see *e.g.* [27–35]. However, now there is a need for high statistics Dalitz plot distributions of $\eta \rightarrow \pi^+\pi^-\pi^0$ to test and/or constrain the theory predictions.

With the radiative decay $J/\psi \rightarrow \gamma\eta$, a clean sample of 8×10^4 $\eta \rightarrow \pi^+\pi^-\pi^0$ candidate events was selected at BESIII. Figure 1(a) shows the $\pi^+\pi^-\pi^0$ invariant mass, with the pronounced η peak and $\sim 0.1\%$ background.

The two Dalitz plot variables are defined as $X = \sqrt{3}(T_{\pi^+} - T_{\pi^-})/Q$ and $Y = 3T_{\pi^0}/Q - 1$, where T_π denotes the kinetic energy of a pion in the η rest frame and $Q = m_\eta - m_{\pi^+} - m_{\pi^-} - m_{\pi^0}$ is the excess energy of the reaction. The distributions of X and Y are shown in Figs. 1 (b) and (c). Using the same parameterization as

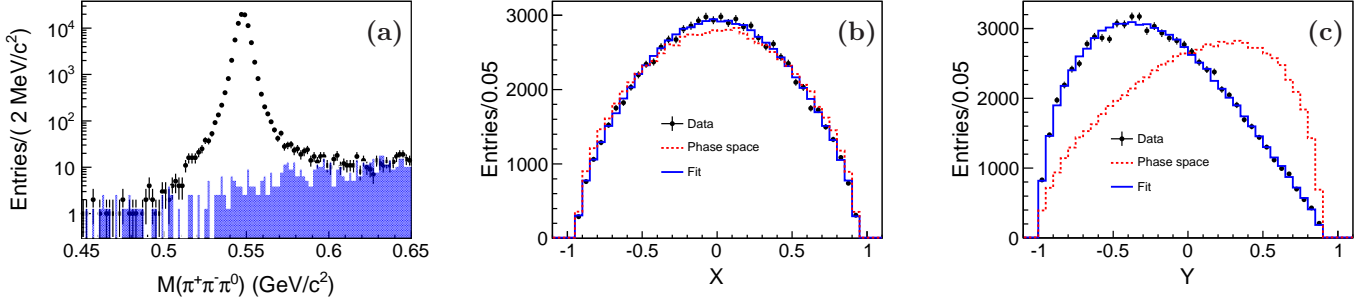


Fig. 1. (a) Distribution of $\pi^+\pi^-\pi^0$ invariant mass. Projections of the Dalitz plot as a function of (b) X and (c) Y for $\eta \rightarrow \pi^+\pi^-\pi^0$ obtained from data (dots with error bars), the fit projections (solid line) and phase space distributed MC events (dashed line).

in Ref. [36], the decay amplitude squared is expressed as

$$|A(X, Y)|^2 \propto 1 + aY + bY^2 + cX + dX^2 + eXY + fY^3 + \dots, \quad (1)$$

where the coefficients a, b, c, \dots are the Dalitz plot parameters. Terms with odd powers of X (c and e parameters) are included only to test charge conjugation (C) conservation. An unbinned maximum likelihood fit to data gives the Dalitz plot parameters shown in Table. 3 where they are compared to the results from previous measurements and theoretical calculations. The effect of including c and e parameters was tested in an alternative fit. The a, b, d and f parameters are almost unchanged, while the parameters c and e are consistent with zero within one standard deviation.

For $\eta \rightarrow \pi^0\pi^0\pi^0$, the amplitude squared is nearly constant and the deviation can be parameterized in the lowest order using just one variable $Z = \frac{2}{3} \sum_{i=1}^3 (3T_i/Q - 1)^2$, where $Q = m_\eta - 3m_{\pi^0}$ and T_i denotes the kinetic energy of each π^0 in the η rest frame. The Dalitz plot density distribution could be parameterized using a linear term,

$$|A(Z)|^2 \propto 1 + 2\alpha Z + \dots, \quad (2)$$

where α is the slope parameter.

The $\pi^0\pi^0\pi^0$ mass spectrum is shown in Fig. 2(a), with the η peak and the background estimated to be less than 1%. The distribution of the variable Z is displayed in Fig. 2(b). Due to the kinematic boundaries and the cusp at the $\pi^0\pi^0 \rightarrow \pi^+\pi^-$ threshold [31, 43], only the interval of $0 < Z < 0.7$ is used to extract the slope parameter α from the data. In analogy to the $\eta \rightarrow \pi^+\pi^-\pi^0$ measurement an unbinned maximum likelihood fit, as displayed in the inset of Fig. 2(b), yields the Dalitz plot slope parameter $\alpha = -0.055 \pm 0.014 \pm 0.004$, which is compatible with the recent results from other experiments.

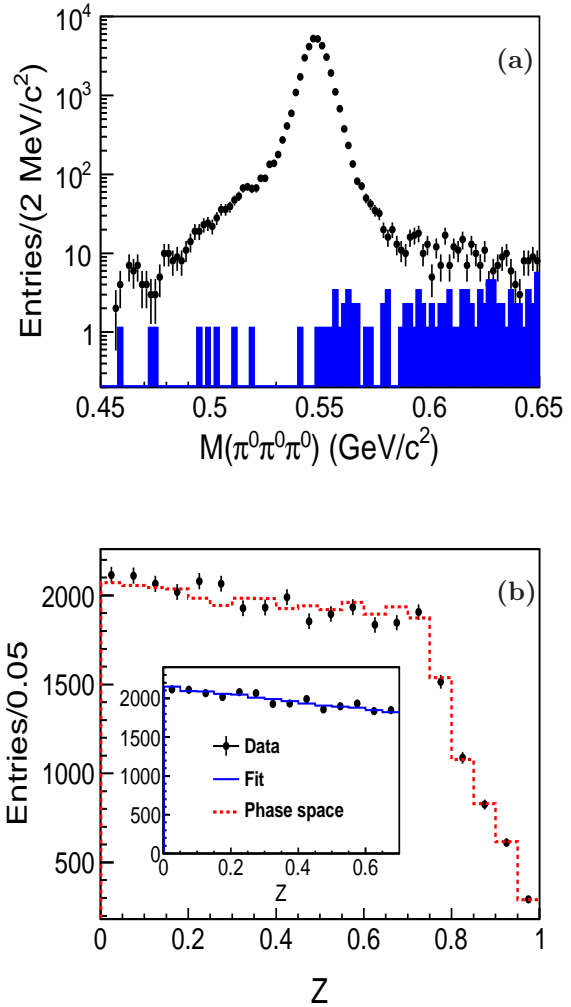


Fig. 2. (a) Distribution of $M(\pi^0\pi^0\pi^0)$ in the η mass region. (b) Distribution of the variable Z for $\eta \rightarrow \pi^0\pi^0\pi^0$. Dots with error bars are for data, histograms for background contributions, dashed histograms for phase space distributed MC events and the solid lines in the inset are the results of the fit.

Table 3. Theoretical and experimental values for the $\eta \rightarrow \pi^+ \pi^- \pi^0$ Dalitz plot parameters.

| Theory/Exp. | a | b | d | f |
|-------------------------|------------------------------|-------------------------------------|-------------------------------------|-------------------------------------|
| ChPT NLO[27] | -1.33 | 0.42 | 0.08 | 0 |
| ChPT NNLO[30] | -1.271 ± 0.075 | 0.394 ± 0.102 | 0.055 ± 0.057 | 0.025 ± 0.160 |
| Dispersive Theory[28] | -1.16 | 0.26 | 0.10 | 0 |
| Absolute Dispersive[37] | -1.21 | 0.33 | 0.04 | 0 |
| UA[38] | -1.049 ± 0.025 | 0.178 ± 0.019 | 0.079 ± 0.028 | 0.064 ± 0.012 |
| NREFT[31] | -1.218 ± 0.013 | 0.314 ± 0.023 | 0.051 ± 0.003 | 0.084 ± 0.019 |
| Layter[39] | -1.08 ± 0.014 | 0.03 ± 0.03 | 0.05 ± 0.03 | - |
| CBarrel[40] | -1.22 ± 0.07 | 0.22 ± 0.11 | $0.06(\text{fixed})$ | - |
| KLOE08[36] | $-1.09^{+0.013}_{-0.024}$ | 0.124 ± 0.016 | $0.057^{+0.016}_{-0.022}$ | 0.14 ± 0.03 |
| WASA-at-COSY[41] | -1.144 ± 0.018 | $0.219 \pm 0.019 \pm 0.047$ | $0.086 \pm 0.018 \pm 0.015$ | 0.115 ± 0.037 |
| BESIII[20] | $-1.128 \pm 0.015 \pm 0.008$ | $0.153 \pm 0.017 \pm 0.004$ | $0.085 \pm 0.016 \pm 0.009$ | $0.173 \pm 0.028 \pm 0.021$ |
| KLOE16[42] | $-1.104 \pm 0.003 \pm 0.002$ | $0.142 \pm 0.003^{+0.005}_{-0.004}$ | $0.073 \pm 0.003^{+0.004}_{-0.003}$ | $0.154 \pm 0.006^{+0.004}_{-0.005}$ |

 Table 4. Theoretical and experimental values for $\eta \rightarrow \pi^0 \pi^0 \pi^0$ Dalitz plot slope parameter α .

| Theory/Exp. | α |
|------------------|--|
| ChPT/NLO[27] | 0.015 |
| dispersive[28] | $(-0.014) - (-0.007)$ |
| UA[38] | -0.031 ± 0.003 |
| ChPT/NNLO[30] | 0.013 ± 0.032 |
| KLOE[44] | $-0.0301 \pm 0.0035^{+0.0022}_{-0.0035}$ |
| WASA-at-COSY[45] | $-0.027 \pm 0.008 \pm 0.005$ |
| CBall[46] | $-0.0322 \pm 0.0012 \pm 0.0022$ |
| SND[47] | $-0.010 \pm 0.021 \pm 0.010$ |
| CBarrel[48] | $-0.052 \pm 0.017 \pm 0.010$ |
| GAM2[49] | -0.022 ± 0.023 |
| BESIII[20] | $-0.055 \pm 0.014 \pm 0.004$ |

2.2 $\eta' \rightarrow \pi^+ \pi^- \eta$ [50] and $\eta' \rightarrow \pi^{+(0)} \pi^{-(0)} \eta$ [51]

The combined branching fraction of the two main hadronic decays of η' : $\eta' \rightarrow \pi^+ \pi^- \eta$ and $\eta' \rightarrow \pi^0 \pi^0 \eta$ is nearly 2/3. The ratio $\mathcal{B}(\eta' \rightarrow \pi^+ \pi^- \eta) / \mathcal{B}(\eta' \rightarrow \pi^0 \pi^0 \eta)$ should be exactly two in the isospin limit. The decays involve both η and pions in the final state and therefore allows to extract information about $\pi\eta$ interactions. However, the excess energy of the processes is relatively small: 130 MeV and 140 MeV for $\pi^+ \pi^- \eta$ and $\pi^0 \pi^0 \eta$ respectively. This means precision high statistics experimental studies of the Dalitz plots together with an appropriate theory framework for extraction of the $\pi\eta$ phase shifts are needed.

The two Dalitz plot variables, X and Y , are usually defined as $X = \frac{\sqrt{3}}{Q}(T_{\pi^+} - T_{\pi^-})$ and $Y = \frac{m_{\eta} + 2m_{\pi}}{m_{\pi}} \frac{T_{\eta}}{Q} - 1$, where $T_{\pi, \eta}$ denote the kinetic energies of the mesons in the η' rest frame and $Q = T_{\eta} + T_{\pi^+} + T_{\pi^-} = m_{\eta'} - m_{\eta} - 2m_{\pi}$.

Two different parametrizations of the Dalitz plot distribution are used. The historically first one assumes a linear amplitude in Y variable:

$$|A(X, Y)|^2 \propto |1 + \alpha Y|^2 + cX + dX^2, \quad (3)$$

the other representation is just a general polynomial expansion:

$$|A(X, Y)|^2 \propto 1 + aY + bY^2 + cX + dX^2, \quad (4)$$

where, α is complex and a, b, c, d are real parameters. These two representations are equivalent in case of $b > a^2/4$.

Initial BESIII $\eta' \rightarrow \pi^+ \pi^- \eta$ Dalitz plot analysis [50] was based on 2009 data and the above two representations was used. The extracted parameters are generally consistent with the previous measurements and theoretical predictions. The negative value of b parameter indicates, with an uncertainty of 30%, that the two representations may not be equivalent. The most recent BESIII analysis [51] uses nearly background free samples of 3.5×10^5 $\eta' \rightarrow \eta \pi^+ \pi^-$ events and 5.6×10^4 $\eta' \rightarrow \eta \pi^0 \pi^0$ events from 1.31×10^9 J/ψ . The goal was determination of the Dalitz plot parameters for the two decay modes and a search for the cusp at the $\pi^0 \pi^0 \rightarrow \pi^+ \pi^-$ threshold in $\eta' \rightarrow \eta \pi^0 \pi^0$. And the fit results for the above two representations, which are shown in Fig. 3 and Fig. 4, and the corresponding fitted parameters are summarized in Table 5.

For the $\eta' \rightarrow \eta \pi^+ \pi^-$ decay, the results, superseding the previous BESIII measurement [50], are not consistent with the measurement from VES and the theoretical predictions within the framework of $U(3)$ chiral effective field theory in combination with a relativistic coupled-channels method (Chiral Unitary Approach -

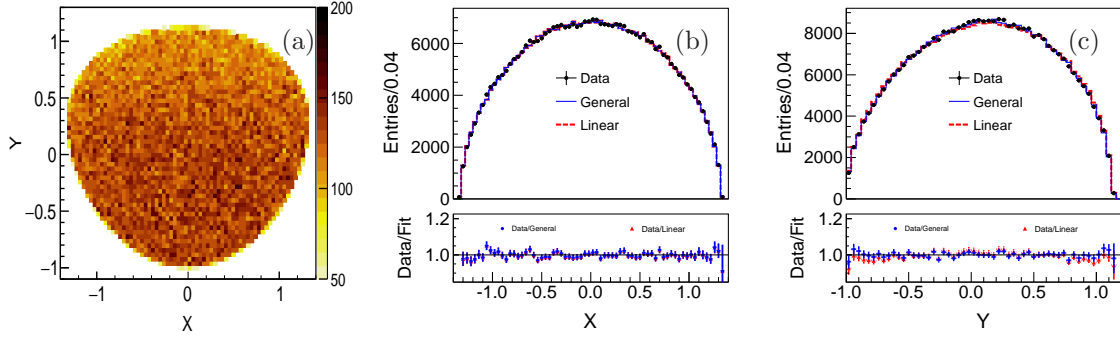


Fig. 3. (a) The experimental Dalitz plot for the decay $\eta' \rightarrow \pi^+\pi^-\eta$ in terms of the variables X and Y with the $\pi^+\pi^-\eta$ mass in the η' mass region. The corresponding projections on variables X and Y are shown in (b) and (c), respectively, where the dashed histograms are from MC of $\eta' \rightarrow \pi^+\pi^-\eta$ events generated with phase space. The solid histograms are the fit results described in the text.

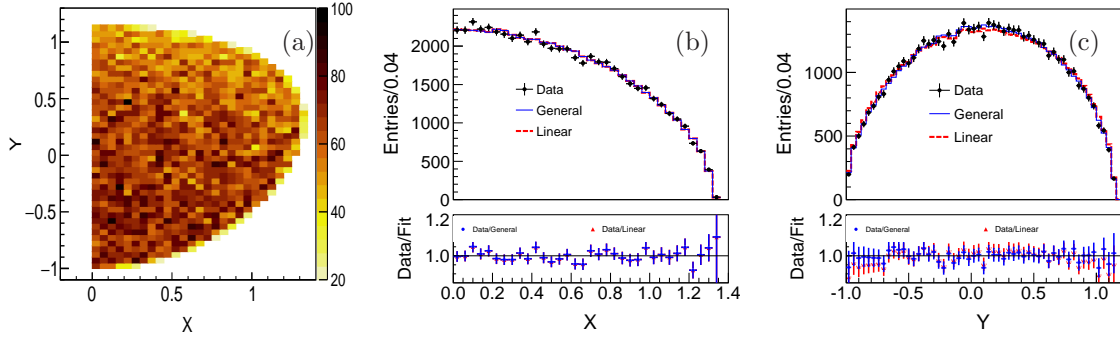


Fig. 4. (a) The experimental Dalitz plot for the decay $\eta' \rightarrow \pi^0\pi^0\eta$ in terms of the variables X and Y with the $\pi^+\pi^-\eta$ mass in the η' mass region. The corresponding projections on variables X and Y are shown in (b) and (c), respectively, where the dashed histograms are from MC of $\eta' \rightarrow \pi^0\pi^0\eta$ events generated with phase space. The solid histograms are the fit results described in the text.

Table 5. Experimental and theoretical values of the Dalitz plot parameters for $\eta' \rightarrow \eta\pi^+\pi^-$ and $\eta' \rightarrow \eta\pi^0\pi^0$. The values for parameter c and $\Im(\alpha)$ are given only for comparison with previous experiments.

| Para. | $\eta' \rightarrow \eta\pi^+\pi^-$ | | | | $\eta' \rightarrow \eta\pi^0\pi^0$ | | |
|---------------|------------------------------------|--------------------|--------------------|--|------------------------------------|--------------------|------------------------------|
| | ChUA [38] | Large N_C [52] | VES [53] | BESIII [51] | ChUA [38] | GAMS-4 π [54] | BESIII [51] |
| hline a | -0.116 ± 0.011 | -0.098 ± 0.048 | -0.127 ± 0.018 | $-0.056 \pm 0.004 \pm 0.003$ | -0.127 ± 0.009 | -0.067 ± 0.016 | $-0.087 \pm 0.009 \pm 0.006$ |
| b | -0.042 ± 0.034 | -0.050 ± 0.001 | -0.106 ± 0.032 | $-0.049 \pm 0.006 \pm 0.006$ | -0.049 ± 0.036 | -0.064 ± 0.029 | $-0.073 \pm 0.014 \pm 0.005$ |
| c | ... | ... | $+0.015 \pm 0.018$ | $(2.7 \pm 2.4 \pm 1.8) \times 10^{-3}$ | ... | ... | ... |
| d | $+0.010 \pm 0.019$ | -0.092 ± 0.008 | -0.082 ± 0.019 | $-0.063 \pm 0.004 \pm 0.004$ | $+0.011 \pm 0.021$ | -0.067 ± 0.020 | $-0.074 \pm 0.009 \pm 0.004$ |
| $\Re(\alpha)$ | ... | ... | -0.072 ± 0.014 | $-0.034 \pm 0.002 \pm 0.002$ | ... | -0.042 ± 0.008 | $-0.054 \pm 0.004 \pm 0.001$ |
| $\Im(\alpha)$ | ... | ... | 0.000 ± 0.100 | $0.000 \pm 0.019 \pm 0.001$ | ... | 0.000 ± 0.070 | $0.000 \pm 0.038 \pm 0.002$ |
| c | ... | ... | $+0.020 \pm 0.019$ | $(2.7 \pm 2.4 \pm 1.5) \times 10^{-3}$ | ... | ... | ... |
| d | ... | ... | -0.066 ± 0.034 | $-0.053 \pm 0.004 \pm 0.004$ | ... | -0.054 ± 0.019 | $-0.061 \pm 0.009 \pm 0.006$ |

ChUA) [38]. In particular for the coefficient a , the discrepancies are about four standard deviations. On the other hand large- N_C ChPT prediction at next-to-next-to-leading order [52] is consistent with the measured a value due to the large theoretical uncertainty. For the coefficient c violating charge conjugation, the fitted values are consistent with zero within one standard deviation for both representations.

In case of $\eta' \rightarrow \eta\pi^0\pi^0$, the results are in general consistent with the previous measurements and theoretical predictions within the uncertainties from both sides. The latest results [55] reported by the A2 experiment are also in agreement with those obtained from BESIII. We notice a discrepancy of 2.6 standard deviations for parameter a between $\eta' \rightarrow \eta\pi^+\pi^-$ and $\eta' \rightarrow \eta\pi^0\pi^0$ modes. The present results are not precise enough to firmly establish isospin violation and additional effects, *e.g.*, radiative corrections [56] and π^+/π^0 mass difference should be considered in the future experimental and theoretical studies.

It was also found that the linear representation could not describe data. The discrepancies between data and the fit are evident in the Y projection for the both decay modes, which is yet another indication that the linear and general representations are not equivalent. In addition, a search for the cusp in $\eta' \rightarrow \eta\pi^0\pi^0$ performed by inspecting the $\pi^0\pi^0$ mass spectrum close to $\pi^+\pi^-$ mass threshold, reveals no statistically significant effect. Most recent theoretical dispersive analysis of the cusp in the $\eta' \rightarrow \eta\pi^0\pi^0$ [57] uses Dalitz plot parameters from VES and 2009 BESIII[50] $\eta' \rightarrow \eta\pi^+\pi^-$ data. However, the amplitudes from Ref. [57] should be preferably fitted directly to the Dalitz plot data for the two decay modes.

2.3 $\eta' \rightarrow \pi^0\pi^0\pi^0$ [20]

The isospin violating decay of $\eta' \rightarrow \pi^0\pi^0\pi^0$ was first observed in $\pi^-p \rightarrow \eta n$ [58]. In a later experiment the Dalitz plot slope parameter was extracted to be $\alpha = -0.1 \pm 0.3$ with limited statistics of around 60 events [59], and in 2008 GAMS-4 π analysis updated to $\alpha = -0.59 \pm 0.18$ using 235 ± 45 events [54]. Using the 2009 J/ψ data sample BESIII has reported the branching fraction of the decay which is about two times larger than Ref. [54, 58, 59] (average $\mathcal{B} = (1.77 \pm 0.23) \times 10^{-3}$ for the three experiments). However, in this first BESIII analysis the Dalitz plot slope parameter was not reported [60].

With the full J/ψ data set a determination of the Dalitz plot slope was possible [20]. The η' signal is clearly observed in $\pi^0\pi^0\pi^0$ mass spectrum, Fig. 5(a), where the hatched and shaded histograms show the background contributions from the inclusive J/ψ decays and $\eta' \rightarrow \pi^0\pi^0\eta$, respectively. As shown in Fig. 5(b), a maximum-likelihood fit to the events with Z in the region

of $0.2 < Z < 0.6$ gives the Dalitz plot slope parameter: $\alpha = -0.640 \pm 0.046 \pm 0.047$, much more precise than previous measurements as summarized in Table. 6. The value deviates significantly from zero, which implies that final state interactions play an important role. Up to now, there are only few theory predictions to compare the parameter value. One exception are the ChUA calculations of Ref. [38]. The predicted value of the α coefficient is in the -2.7 to 0.1 range, consistent with the BESIII measurement.

Table 6. Theoretical and experimental values for $\eta' \rightarrow \pi^0\pi^0\pi^0$ Dalitz plot slope parameter α .

| Theory/Exp. | α |
|-------------|------------------------------|
| ChUA[38] | $-2.7 \sim 0.1$ |
| GAMS[54] | -0.59 ± 0.18 |
| GAM2[59] | -0.1 ± 0.3 |
| BESIII[20] | $-0.640 \pm 0.046 \pm 0.047$ |

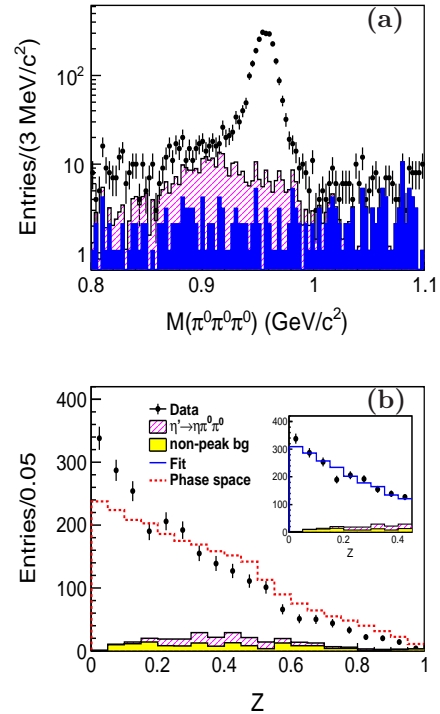


Fig. 5. (a) Distribution of $M(\pi^0\pi^0\pi^0)$ in the η' mass region. (b) Distribution of the variable Z for $\eta' \rightarrow \pi^0\pi^0\pi^0$. Dots with error bars are for data, histograms for background contributions, dashed histograms for phase space distributed MC events and the solid lines in the inset are the results of the fit.

2.4 Amplitude analysis of $\eta' \rightarrow \pi^{+(0)}\pi^{-(0)}\pi^0$ [11]

At first, the low intensity process $\eta' \rightarrow \pi^+\pi^-\pi^0$ may be considered to come from $\pi^0 - \eta$ mixing in the domi-

nating decay $\eta' \rightarrow \pi^+\pi^-\eta$ [61]. This would offer a possibility to determine precisely $u-d$ quark mass difference from the branching fraction ratio of the two processes. However, a recent analysis shows that even at tree level other terms are needed [62]. In addition the decay amplitudes are strongly affected by the intermediate resonances. Therefore the mixing of $\pi^0-\eta$ and $u-d$ quark mass difference cannot be extracted in a simple way.

The decay $\eta' \rightarrow \pi^+\pi^-\pi^0$ was first observed by the CLEO experiment [63] in 2008. BESIII has reported the branching fraction measurement using 2009 J/ψ data set [60] but the amplitude analysis was only possible with the full data set. In particular it was expected that contribution of $\eta' \rightarrow \rho^\pm\pi^\mp$ could be identified. This expectation is supported by the experimental distributions shown in the Dalitz plot of $M^2(\pi^+\pi^-)$ versus $M^2(\pi^-\pi^0)$ in Fig. 6, where the two clusters corresponding to the contribution $\eta' \rightarrow \rho^\pm\pi^\mp$ are seen.

The common amplitude analysis of the decays $\eta' \rightarrow \pi^+\pi^-\pi^0$ and $\eta' \rightarrow \pi^0\pi^0\pi^0$ is performed using isobar model. The fit results illustrated by the invariant mass spectra of $\pi^+\pi^-$, $\pi^+\pi^0$ and $\pi^-\pi^0$ (Fig. 7) show significant P -wave contribution from $\eta' \rightarrow \rho^\pm\pi^\mp$ in $\eta' \rightarrow \pi^+\pi^-\pi^0$. The branching fraction $\mathcal{B}(\eta' \rightarrow \rho^\pm\pi^\mp)$ is determined to be $(7.44 \pm 0.60 \pm 1.26 \pm 1.84_{\text{model}}) \times 10^{-4}$. In addition to the non-resonant S -wave, the resonant π - π S -wave with a pole at $(512 \pm 15) - i(188 \pm 12)$ MeV, interpreted as the broad σ meson, plays essential role in the $\eta' \rightarrow \pi\pi\pi$ decays. Due to the large interference between non-resonant and resonant S -waves, only the sum is used to describe the S -wave contribution, and the branching fraction is determined to be $\mathcal{B}(\eta' \rightarrow \pi^+\pi^-\pi^0)_S = (37.63 \pm 0.77 \pm 2.22 \pm 4.48_{\text{model}}) \times 10^{-4}$.

For $\eta' \rightarrow \pi^0\pi^0\pi^0$, the P -wave contribution in two-body rescattering is forbidden by Bose symmetry. The Dalitz plot for $\eta' \rightarrow \pi^0\pi^0\pi^0$ is shown in Fig. 8 (a) and the amplitude fit is displayed in Fig. 8 (b). The corresponding branching fraction is measured to be $\mathcal{B}(\eta' \rightarrow \pi^0\pi^0\pi^0) = (35.22 \pm 0.82 \pm 2.60) \times 10^{-4}$.

The branching fractions of $\eta' \rightarrow \pi^+\pi^-\pi^0$ and $\eta' \rightarrow \pi^0\pi^0\pi^0$ are in good agreement with and supersede the previous BESIII measurements [60]. The value for $\mathcal{B}(\eta' \rightarrow \pi^0\pi^0\pi^0)$ is two times larger than GAMS measurement of $(16 \pm 3.2) \times 10^{-4}$ [59]. The significant resonant S -wave contribution also provides a reasonable explanation for the negative slope parameter of the $\eta' \rightarrow \pi^0\pi^0\pi^0$ Dalitz plot [20]. The ratio between the S -wave components of the two decay modes, $\mathcal{B}(\eta' \rightarrow \pi^0\pi^0\pi^0)/\mathcal{B}(\eta' \rightarrow \pi^+\pi^-\pi^0)_S$, is determined to be $0.94 \pm 0.029 \pm 0.13$, where the common systematic cancels. With the branching fractions of $\eta' \rightarrow \pi\pi\eta$ taken from Particle Data Group (PDG) [17], $r_\pm = \mathcal{B}(\eta' \rightarrow \pi^+\pi^-\pi^0)/\mathcal{B}(\eta' \rightarrow \pi^+\pi^-\eta)$ and $r_0 = \mathcal{B}(\eta' \rightarrow \pi^0\pi^0\pi^0)/\mathcal{B}(\eta' \rightarrow \pi^0\pi^0\eta)$ are calculated to be $(8.8 \pm 1.2) \times 10^{-3}$ and $(16.9 \pm 1.4) \times 10^{-3}$, respectively.

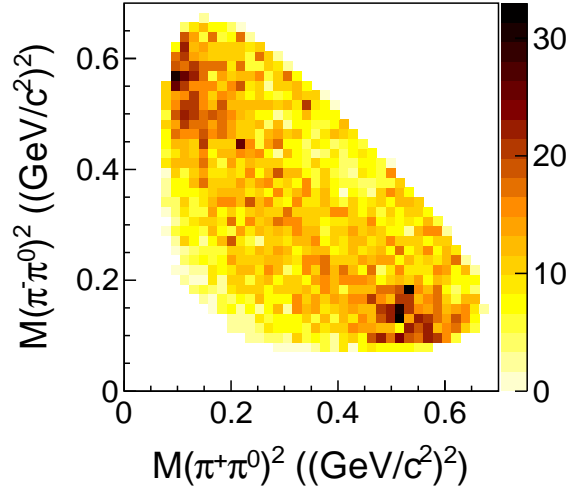


Fig. 6. Dalitz plot of $M^2(\pi^+\pi^0)$ versus $M^2(\pi^-\pi^0)$ for $\eta' \rightarrow \pi^+\pi^-\pi^0$ candidate events selected from data.

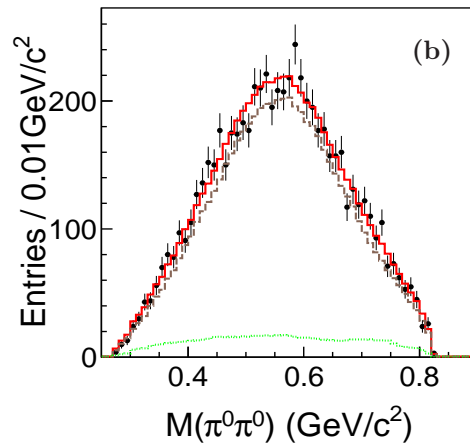
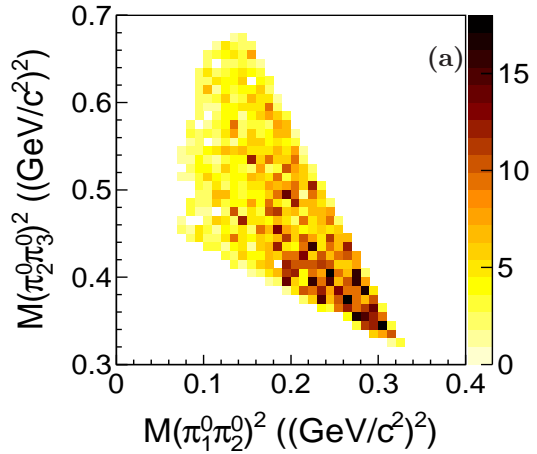


Fig. 8. (a) $\eta' \rightarrow \pi^0\pi^0\pi^0$ Dalitz plot for candidate events selected from data. (b) Comparison of $\pi^0\pi^0$ mass spectrum between data (dots

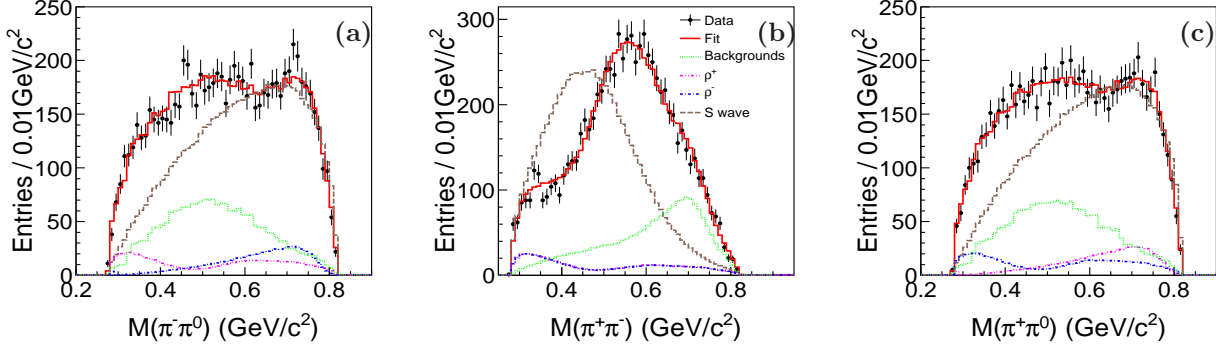


Fig. 7. Comparison of the invariant mass distributions of (a) $\pi^- \pi^0$, (b) $\pi^+ \pi^-$, (c) $\pi^+ \pi^0$ (dots with error bars) and the fit projections (solid histograms). The dotted, dashed, dash-dotted, and dash-dot-dotted histograms show the contributions from background, S wave, ρ^- , and ρ^+ , respectively.

with error bars) and the fit projections (solid histograms).

2.5 $\eta' \rightarrow \pi^+ \pi^- \pi^+ \pi^-, \pi^+ \pi^- \pi^0 \pi^0$ [15]

In ChPT anomalous hadronic decays $\eta' \rightarrow \pi^+ \pi^- \pi^+ \pi^-$ are related to WZW pentagon contribution. In the VMD model $\rho^0 \rho^0$ or $\rho^+ \rho^-$ intermediate state should provide dominant contribution. Using a combination of ChPT and VMD the branching fractions were calculated to be $\mathcal{B}(\eta' \rightarrow \pi^+ \pi^- \pi^+ \pi^-) = (1.0 \pm 0.3) \times 10^{-4}$ and $\mathcal{B}(\eta' \rightarrow \pi^+ \pi^- \pi^0 \pi^0) = (2.4 \pm 0.7) \times 10^{-4}$ [64].

The $\pi^+ \pi^- \pi^+ \pi^-$ invariant mass distributions for the BESIII analysis are shown in Figs. 9(a) and (b), respectively, where the η' peak is clearly seen. The results of background simulations are indicated by the hatched histograms in Figs. 9(a) and (b). None of the background sources produces a peak in the $\pi^+ \pi^- \pi^+ \pi^-$ invariant mass spectrum near the η' mass.

In order to measure the branching fractions, the signal efficiency was estimated using a signal MC sample using two assumptions: the flat phase space and the decay amplitudes from Ref. [64]. For $\eta' \rightarrow \pi^+ \pi^- \pi^+ \pi^-$, each of the $M(\pi^+ \pi^-)$ combinations was divided into 38 bins in the region of $[0.28, 0.66]$ GeV/ c^2 . With the procedure described above, the number of the η' events in each bin is obtained by fitting the $\pi^+ \pi^- \pi^+ \pi^-$ mass spectrum in this bin, and then the background-subtracted $M(\pi^+ \pi^-)$ is obtained as shown in Fig. 9 (c) (four entries per event), where the errors are statistical only. The comparison of the experimental $M(\pi^+ \pi^-)$ distribution and two models is shown in Fig. 9(c). The amplitude of Ref. [64] provides better description of the data than the phase space. Therefore this amplitude is used in the simulation to determine the detection efficiency for $\eta' \rightarrow \pi^+ \pi^- \pi^+ \pi^-$ decays.

The signal yields are obtained from extended unbinned maximum likelihood fits to the $\pi^+ \pi^- \pi^+ \pi^-$ and $\pi^+ \pi^- \pi^0 \pi^0$ invariant mass distributions and the statisti-

cal significances for $\eta' \rightarrow \pi^+ \pi^- \pi^+ \pi^-$ and $\eta' \rightarrow \pi^+ \pi^- \pi^0 \pi^0$ are calculated to be 18σ and 5σ , respectively. The branching fractions of $\eta' \rightarrow \pi^+ \pi^- \pi^+ \pi^-$ are determined to be $\mathcal{B}(\eta' \rightarrow \pi^+ \pi^- \pi^+ \pi^-) = (8.53 \pm 0.69 \pm 0.64) \times 10^{-5}$ and $\mathcal{B}(\eta' \rightarrow \pi^+ \pi^- \pi^0 \pi^0) = (1.82 \pm 0.35 \pm 0.18) \times 10^{-4}$, which are in agreement with the predictions in Ref. [64], but not with an older estimate based on broken- $SU(6) \times O(6)$ quark model [65].

3 Radiative and Dalitz decays

3.1 $\eta' \rightarrow \pi^+ \pi^- \gamma$ (preliminary results)

The anomalous process $\eta' \rightarrow \gamma \pi^+ \pi^-$ is the second most probable decay of the η' meson ($\mathcal{B} = 29.1 \pm 0.5$ % [17]) and frequently used for η' tagging. In the VMD model the main contribution to the decay comes from $\eta' \rightarrow \gamma \rho^0$ [66]. In the past the di-pion mass distribution was studied by several experiments *e.g.* JADE [67], CELLO [68], PLUTO [69], TASSO [70], TPC/ $\gamma\gamma$ [71], and ARGUS [72]. A peak shift of about +20 MeV with respect to the expected position from the ρ^0 contribution was consistently observed. Dedicated [73] analysis using ~ 2000 $\eta' \rightarrow \gamma \pi^+ \pi^-$ events concluded that ρ^0 contribution is not sufficient to describe the di-pion mass spectrum. This discrepancy could be attributed to the WZW box anomaly contribution which should be included as an extra non resonant term in the decay amplitude. It was suggested that the fits to the shape of the di-pion distribution will allow to determine the ratio of the two contributions [74]. The evidence for the box anomaly with a significance of 4σ was reported in 1997 by the Crystal Barrel experiment [75] using a sample of 7490 ± 180 η' events but this observation was not confirmed by the subsequent measurement by the L3 Collaboration [76] using 2123 ± 53 events. Recently proposed model-independent approach, based on ChPT and a dispersion theory, describes the $\eta/\eta' \rightarrow \pi^+ \pi^- \gamma$ decay amplitudes as a product of an universal and a reaction specific part [77]. The uni-

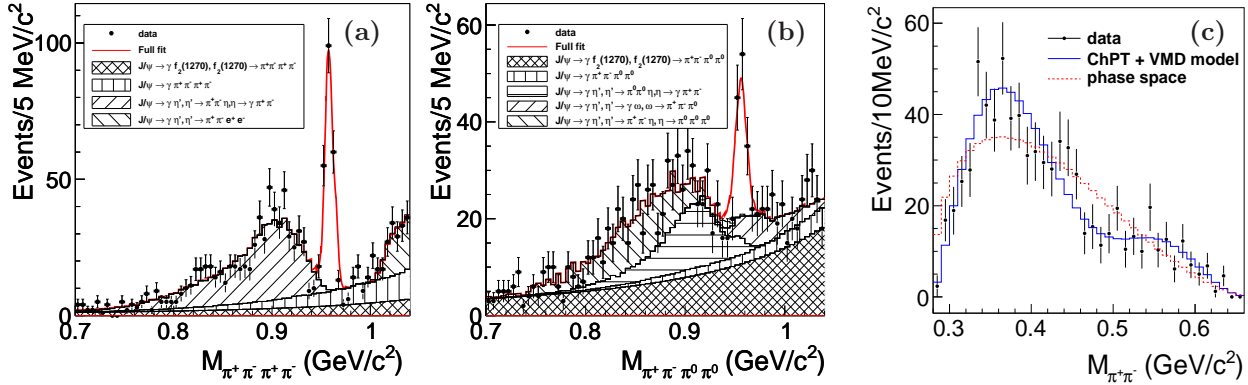


Fig. 9. Results of the fits to (a) $M(\pi^+\pi^-\pi^+\pi^-)$, (b) $M(\pi^+\pi^-\pi^0\pi^0)$ and (c) $M(\pi^+\pi^-)$, where the background contributions are displayed as the hatched histograms.

versal part could be extracted from the pion vector form factor measured precisely in $e^+e^- \rightarrow \pi^+\pi^-$. The reaction specific part was determined experimentally for the $\eta \rightarrow \pi^+\pi^-\gamma$ decay by WASA-at-COSY [78] and KLOE [79]. It was shown the di-pion distribution for the η decay can not be described by the pion vector form factor only. In Ref. [80] it was hypothesized that the reaction specific part could be similar for the η and η' decays.

For BESIII analysis a low background data sample of 9.7×10^5 $\eta' \rightarrow \gamma\pi^+\pi^-$ decays candidates is selected. The distribution of the $\pi^+\pi^-$ invariant mass, $M(\pi^+\pi^-)$, is displayed in Fig. 10. The $\rho^0 - \omega$ interference is seen for first time in this decay. In the model-dependent approach the data can not be described with Gounaris-Sakurai parameterisation [81] of the ρ^0 and the ω contributions including the interference. The fit performance gets much better after including the box anomaly, Fig. 10(a), with a statistical significance larger than 37σ . An alternative fit was performed by replacing the box anomaly with $\rho^0(1450)$, Fig. 10(b), by fixing its mass the width to the world average values. The fit is slightly worse but it still provides a reasonable description of the data.

Using model-independent approach of Ref. [77] and including $\rho^0 - \omega$ mixing the pion vector form factor $F_V(s)$ (where $s = M^2(\pi^+\pi^-)$) and amplitudes for $\eta/\eta' \rightarrow \gamma\pi^+\pi^-$ decays are proportional to $P(s) \cdot \Omega(s)$ where $P(s)$ is a reaction specific term, $P(s) = 1 + \kappa s + \lambda s^2 + \xi \cdot BW_\omega + \mathcal{O}(s^4)$, $\Omega(s)$ is the Omnès function describing $\pi - \pi$ interactions with $L = 1$ [80, 82]. For $\eta \rightarrow \gamma\pi^+\pi^-$ only the linear term $\kappa = 1.32 \pm 0.13 \text{ GeV}^{-2}$ [78, 79] is needed. The fit to the BESIII $\eta' \rightarrow \gamma\pi^+\pi^-$ data is shown in Fig. 10(c), it yields $\kappa = 0.992 \pm 0.039 \text{ GeV}^{-2}$, $\lambda = -0.523 \pm 0.039 \text{ GeV}^{-4}$, $\xi = 0.199 \pm 0.006$ with the fit goodness $\chi^2/\text{ndf} = 145/109$. The presence of the quadratic term is consistent with recent calculations including intermediate $\pi^\pm a_2^\mp$ state [83].

3.2 $\eta' \rightarrow \pi^+\pi^-l^+l^-$ [84]

The first observation of the conversion decay $\eta' \rightarrow \pi^+\pi^-e^+e^-$ was reported in 2009 by the CLEO [63] Collaboration. The decay is directly related to $\eta' \rightarrow \pi^+\pi^-\gamma$ and involves virtual photon, $\eta' \rightarrow \pi^+\pi^-\gamma^* \rightarrow \pi^+\pi^-e^+e^-$. The conversion process provides a more stringent test of the models. Predictions for the decay are given within VMD model and unitarized ChPT [85–87]. In the e^+e^- invariant mass ($q \equiv M(e^+e^-)$) distribution for a conversion decay the contribution of the photon propagator translates to the pole-like $1/q$ dependence close to the lower kinematic boundary of $q = 2m_e$ (see also Sec. 3.3). For the $\eta' \rightarrow \pi^+\pi^-e^+e^-$ decay a dominant ρ^0 contribution in the $M(\pi^+\pi^-)$ is also expected. The CLEO measurement based on just $7.9^{+3.9}_{-2.7}$ signal events was unable to explore these distributions. However, the measured branching fraction $\mathcal{B}(\eta' \rightarrow \pi^+\pi^-e^+e^-) = (2.5^{+1.2}_{-0.9} \pm 0.5) \times 10^{-3}$ [63], is consistent with the predicted value of $\sim 2 \times 10^{-3}$. The corresponding conversion decay with a $\mu^+\mu^-$ pair are suppressed by two orders of magnitude due to $q = 2m_\mu$ cutoff. In the CLEO analysis an upper limit of $\mathcal{B}(\eta' \rightarrow \pi^+\pi^-\mu^+\mu^-) < 2.4 \times 10^{-4}$, at 90% C.L. was set.

The finished BESIII analysis is based only on 2009 data. Figure 11 displays the e^+e^- mass spectrum by requiring $|M(\pi^+\pi^-e^+e^-) - m_{\eta'}| < 0.02 \text{ GeV}/c^2$, where the background from $\gamma\pi^+\pi^-$ following the photon conversion in the detector material could be clearly seen. The peak close to $2m_e$ corresponds to the $\eta' \rightarrow \pi^+\pi^-e^+e^-$ signal and the second peak around $0.015 \text{ GeV}/c^2$ comes from the $\eta' \rightarrow \gamma\pi^+\pi^-$ background. For the selected data sample any other background is negligible and the efficiency for the signal is 16.9%. The number of 429 ± 24 signal events is taken from a fit of the two contributions to the $M(e^+e^-)$ distribution. The corresponding branching fraction of $\mathcal{B}(\eta' \rightarrow \pi^+\pi^-e^+e^-) = (2.11 \pm 0.12 \pm 0.15) \times 10^{-3}$ is in good agreement with theoretical predictions and

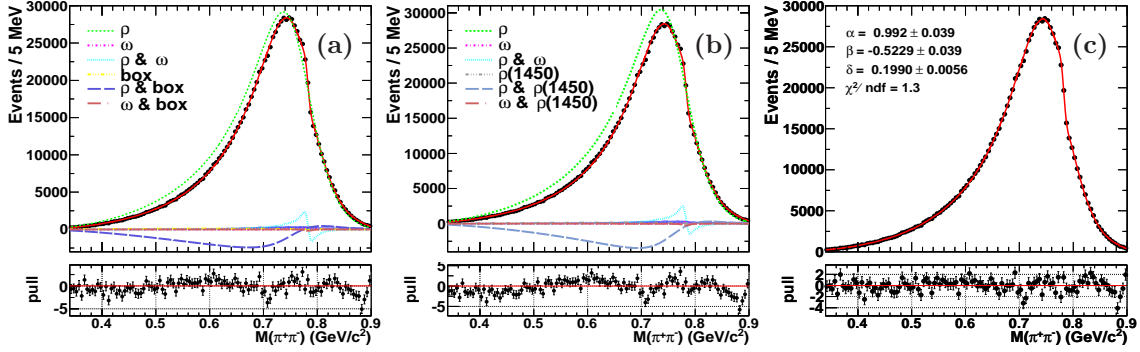


Fig. 10. The results of the model-dependent fits to $M(\pi^+\pi^-)$ with (a) $\rho^0-\omega$ -*box* anomaly and (b) $\rho^0-\omega-\rho^0(1450)$. (c) The results of model-independent fit with ω interference.

with the CLEO result. The mass spectra of $\pi^+\pi^-$ and e^+e^- are consistent with the expected ρ^0 domination in $M(\pi^+\pi^-)$ distribution and the peak in the $M(e^+e^-)$ distribution just above $2m_e$ threshold with a long tail.

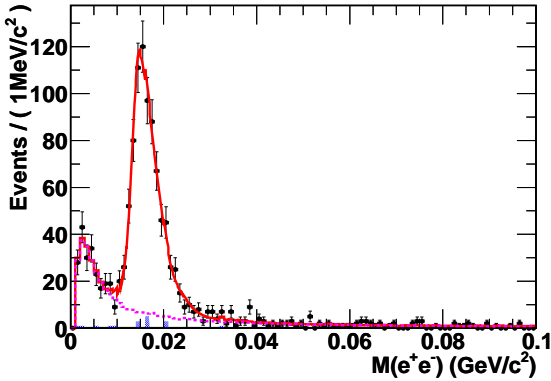


Fig. 11. The invariant mass spectrum of e^+e^- for data (dots with error bars) after all the selection criteria are applied. The solid line represents the fit result, the dotted histogram is MC signal shape and the shaded histogram is for backgrounds obtained from η' sideband events.

Figure 12 shows the invariant mass of $\pi^+\pi^-\mu^+\mu^-$, where no η' signal is observed. The remaining events in the η' mass region are consistent with the contributions from the background estimated with MC simulations. The upper limit of $\mathcal{B}(\eta' \rightarrow \pi^+\pi^-\mu^+\mu^-) < 2.9 \times 10^{-5}$ at the 90% C.L. is set.

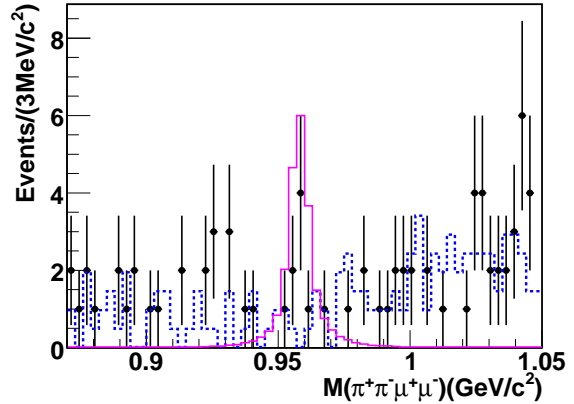


Fig. 12. Invariant mass spectrum of $\pi^+\pi^-\mu^+\mu^-$ for data (dots with error bars) after all the selection criteria are applied. The solid line represents the fit result, the dotted histogram is MC signal shape and the shaded histogram is for backgrounds obtained from η' sideband events.

3.3 $\eta' \rightarrow \gamma e^+e^-$ [12]

Dalitz decays of light pseudoscalar mesons, $P \rightarrow \gamma e^+e^-$ where $P = \pi^0, \eta, \eta'$, play an important role in revealing structure of the hadrons and the interaction mechanism between photons and the hadrons [9]. The decay rates can be calculated in Quantum Electrodynamics (QED) where the inner structure of the mesons is encoded by the transition form factor (TFF), $F(q^2)$, where q^2 is the invariant mass of the lepton pair squared. A recent summary and discussion of this subject can be found in Ref. [88].

The knowledge of the TFF is also important in studies of the muon anomalous magnetic moment, $a_\mu = (g_\mu - 2)/2$, which is one of the most precise low-energy test of the Standard Model and an important probe for new physics. The theoretical uncertainty on the SM calculation of a_μ is dominated by hadronic corrections and therefore limited by the accuracy of their de-

termination [89]. In particular, the hadronic light-by-light (HLbL) scattering contribution to a_μ includes two meson-photon-photon vertices that can be related to the TFF. Thus, models describing these transitions should be tested to reduce the uncertainty in the SM prediction for a_μ .

The conversion decay $\eta' \rightarrow \gamma e^+ e^-$ is closely related to $\eta' \rightarrow \gamma \pi^+ \pi^-$, and in particular the transition form factor could be predicted from the invariant mass distribution of the two pions and the branching ratio of the $\eta' \rightarrow \gamma \pi^+ \pi^-$ decay in a model independent way using a dispersive integral [80].

The differential decay width [9] is calculated with,

$$\frac{d\Gamma(\eta' \rightarrow \gamma l^+ l^-)}{dq^2 \Gamma(\eta' \rightarrow \gamma \gamma)} = [\text{QED}(q^2)] \times |F(q^2)|^2, \quad (5)$$

where $[\text{QED}(q^2)]$ represents the QED part for a point-like meson which includes $1/q^2$ term due to photon propagator. Therefore for conversion decays involving electron-positron pair the distribution peaks at the lowest invariant masses $q = 2m_e$. The TFF can be experimentally determined from the ratio of the measured di-lepton invariant mass spectrum and the $[\text{QED}(q^2)]$ term. In the VMD model, it is assumed that interactions between virtual photon and hadrons are described by a superposition of neutral vector meson states [8, 90]. The dominant contribution is expected to come from ρ^0 meson and the form factor could be described by:

$$F(q^2) = N \frac{m_V^2}{m_V^2 - q^2 - i\Gamma_V m_V}, \quad (6)$$

where N is a factor ensuring that $F(0) = 1$ and $m_V \approx m_\rho$, $\Gamma_V \approx \Gamma_\rho$ where m_ρ , Γ_ρ is the mass and width of the ρ^0 meson respectively. In the case of the η' , the mass of the pole lies within the kinematic boundaries of the decay and therefore the $-i\Gamma_V m_V$ term cannot be neglected. A parameter often extracted experimentally is the slope of the form factor, b , defined as

$$b = \left. \frac{d|F|}{dq^2} \right|_{q^2=0} = \frac{1}{m_V^2 + \Gamma_V^2}. \quad (7)$$

Before the BESIII result, only the $\eta' \rightarrow \gamma \mu^+ \mu^-$ process has been observed with the TFF slope measured to be $b_{\eta'} = (1.7 \pm 0.4) \text{ GeV}^{-2}$ [9, 91]. In the VMD model, $\Gamma(\eta' \rightarrow \gamma e^+ e^-)/\Gamma(\eta' \rightarrow \gamma \gamma) = (2.06 \pm 0.02)\%$ [87] to be compared to 1.8% if the TFF is set to one. The TFF slope is expected to be $b_{\eta'} = 1.45 \text{ GeV}^{-2}$ [92, 93] in the VMD model, while in ChPT it is $b_{\eta'} = 1.60 \text{ GeV}^{-2}$ [94]. A recent calculation based on a dispersion integral gives $b_{\eta'} = 1.53_{-0.08}^{+0.15} \text{ GeV}^{-2}$ [80].

In the BESIII experiment the largest background comes from QED processes and $J/\psi \rightarrow e^+ e^- \gamma \gamma$ decays. For these channels, the combination of the $e^+ e^-$ with

any final-state photon produces a smooth $M(\gamma e^+ e^-)$ distribution. The primary peaking background comes from the decay $\eta' \rightarrow \gamma \gamma$ followed by a γ conversion in the material in front of the main drift chamber. The distance from the reconstructed vertex point of the electron-positron pair to the z axis is used to reduce the background down to 42.7 ± 8.0 events. The resulting $M(\gamma e^+ e^-)$ distribution after the selection criteria is shown in Fig. 13(a) and exhibits a clear peak at the η' mass. A fit is performed to determine the signal yield with the signal shape represented by the MC. The non-peaking background is described by a first-order Chebychev polynomial. The fraction of the peaking background is fixed from the simulation. The signal yield and the detection efficiency is summarized in Table 2. The decay $\eta' \rightarrow \gamma \gamma$ from the same data set is used for normalization and the result is quoted in terms of the ratio $\Gamma(\eta' \rightarrow \gamma e^+ e^-)/\Gamma(\eta' \rightarrow \gamma \gamma) = (2.13 \pm 0.09 \pm 0.07) \times 10^{-2}$. Using the branching fraction of $\eta' \rightarrow \gamma \gamma$ in PDG [17], we obtain the first measurement of the $\eta' \rightarrow \gamma e^+ e^-$ branching fraction reported in Table 2.

The TFF is extracted from the bin-by-bin efficiency corrected signal yields for eight $M(e^+ e^-)$ bins for $M(e^+ e^-) < 0.80 \text{ GeV}/c^2$. The bin widths of 0.1 GeV are used and are much wider than the $M(e^+ e^-)$ resolution (5~6 MeV depending on $M(e^+ e^-)$). The signal yield in each $M(e^+ e^-)$ bin is obtained by repeating the fits to the $M(\gamma e^+ e^-)$ mass distributions.

The result for $|F|^2$ is obtained by dividing the acceptance corrected yields by the integrated QED prediction in each $M(e^+ e^-)$ bin and it is shown in Figs. 13 (b) and (c). The parameters from the fit of the TFF to the parametrization of Eq. 6 are $m_V = (0.79 \pm 0.04 \pm 0.02) \text{ GeV}$ and $\Gamma_V = (0.13 \pm 0.06 \pm 0.03) \text{ GeV}$. The single pole parameterization provides a good description of data as shown in Fig. 13 (b). The corresponding value of the slope parameter is $b_{\eta'} = (1.56 \pm 0.19) \text{ GeV}^{-2}$, in agreement with the result from $\eta' \rightarrow \gamma \mu^+ \mu^-$ [9]. The slope agrees also within errors with the VMD model predictions and the uncertainty matches the best determination in the space-like region from the CELLO collaboration $b_{\eta'} = (1.60 \pm 0.16) \text{ GeV}^{-2}$ [95].

3.4 $\eta' \rightarrow e^+ e^- \omega$ [13]

The decay $\eta' \rightarrow \pi^+ \pi^- e^+ e^-$ [84] is dominated by $\eta' \rightarrow \rho^0 e^+ e^-$, in agreement with theoretical predictions [85, 86]. The corresponding decay $\eta' \rightarrow \omega e^+ e^-$ was not observed before BESIII measurements. Theoretical models [85, 96] predict the branching fraction to be around 2.0×10^{-4} .

A parallel analysis of $\eta' \rightarrow e^+ e^- \omega$ and $\eta' \rightarrow \gamma \omega$ decays allows to reduce the impact of systematic errors for the ratio of the branching fractions. For $\eta' \rightarrow e^+ e^- \omega$ decay, candidate events with four well-reconstructed charged

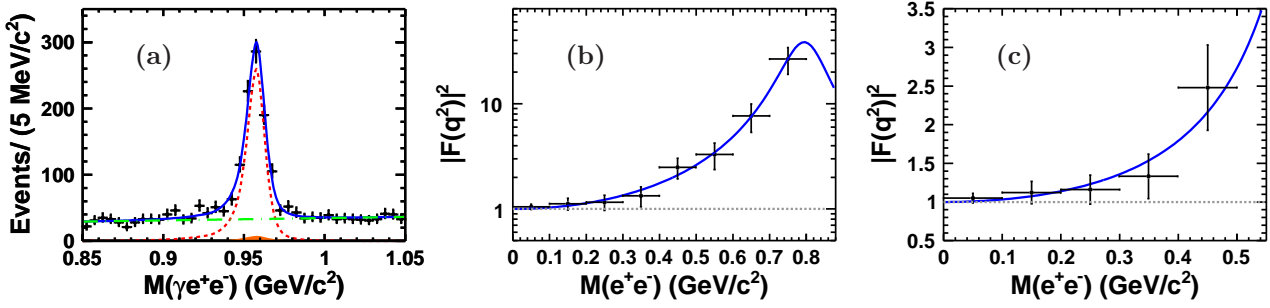


Fig. 13. (a) Invariant $\gamma e^+ e^-$ mass distribution for the selected signal events. The (black) crosses are the data, the (red) dashed line represents the signal, the (green) dot-dashed curve shows the non-peaking background shapes, the (orange) shaded component is the shape of the peaking background events. (b) Fit to the single pole form factor $|F|^2$. (c) Determination of the form factor slope by fitting to $|F|^2$.

tracks and at least three photons are selected. The external conversion background from $\eta' \rightarrow \gamma\omega$ is removed by requiring the distance of the vertex from the z axis to be less than 2 cm (according to simulation only 2.6 ± 0.3 background events will survive the cut). In the selected data sample both the ω peak in $M(\pi^0\pi^+\pi^-)$ and the η' peak in $M(\pi^0\pi^+\pi^-e^+e^-)$ is clearly seen in the scatter plot shown in Fig. 14(a). The best identification of the process is achieved in the $M(\pi^0\pi^+\pi^-e^+e^-) - M(\pi^0\pi^+\pi^-)$ distribution. This distribution is used in a fit to extract the signal yields as indicated in Fig. 14(b). The decay of $\eta' \rightarrow \omega e^+ e^-$ is observed with a statistical significance of 8σ , and its branching fraction is measured to be $\mathcal{B}(\eta' \rightarrow \omega e^+ e^-) = (1.97 \pm 0.34 \pm 0.17) \times 10^{-4}$, consistent with theoretical predictions [85, 96].

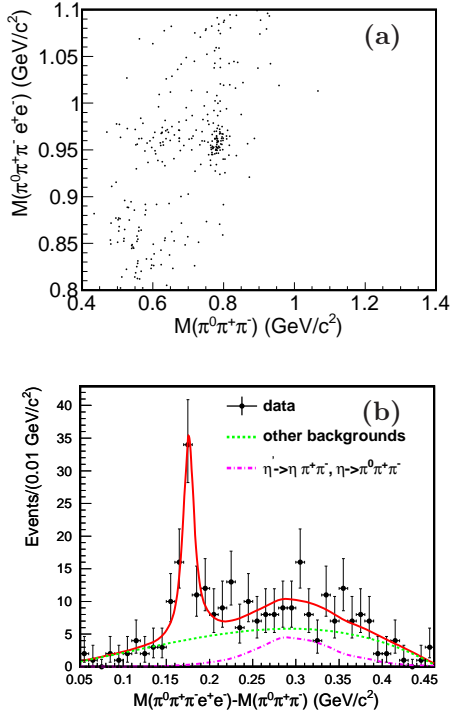


Fig. 14. (a) Distribution of $M(\pi^0\pi^+\pi^-e^+e^-)$

versus $M(\pi^0\pi^+\pi^-)$. (b) Distribution of $M(\pi^0\pi^+\pi^-e^+e^-) - M(\pi^0\pi^+\pi^-)$ with the fit results. The dash-dotted line is the $\eta' \rightarrow \pi^+\pi^-\eta$ background contributions and the dotted line is the remaining background.

3.5 $\eta' \rightarrow \gamma\gamma\pi^0$ [14]

The $\eta' \rightarrow \gamma\gamma\pi^0$ decay should be dominated by the sequential process $\eta' \rightarrow \gamma\omega \rightarrow \gamma\gamma\pi^0$. The interesting question is to determine a non-resonant contribution to the decay. At present there is only a preliminary theoretical analysis which uses combination of the linear sigma model and VMD. The prediction for branching fraction of $\eta' \rightarrow \gamma\gamma\pi^0$ is $\sim 6 \times 10^{-3}$ [97, 98]. This is quite puzzling result giving two times larger value than the $\gamma\omega$ sequence. The first observation of $\eta' \rightarrow \gamma\gamma\pi^0$ is reported by the BESIII experiment. Fig. 15(a) shows the $\gamma\gamma\pi^0$ invariant mass spectrum, where the clear η' peak is observed. By assuming that the inclusive decay $\eta' \rightarrow \gamma\gamma\pi^0$ can be attributed to the vector mesons ρ^0 and ω and the non-resonant contribution, a unbinned maximum likelihood fit to the $\gamma\pi^0$ invariant mass [Fig. 15 (b)] is performed to determine the signal yields for the non-resonant $\eta' \rightarrow \gamma\gamma\pi^0$ decay using the η' signal events with $|M(\gamma\gamma\pi^0) - m_{\eta'}| < 25 \text{ MeV}/c^2$. In the fit, the ρ^0 - ω interference is considered, but possible interference between the ω (ρ^0) and the non-resonant process is neglected.

The branching fraction of the inclusive decay is measured to be $\mathcal{B}(\eta' \rightarrow \gamma\gamma\pi^0)_{\text{Incl.}} = (3.20 \pm 0.07 \pm 0.23) \times 10^{-3}$, which is much lower than the theoretical predictions [97, 98]. In addition, the branching fraction for the non-resonant decay is determined to be $\mathcal{B}(\eta' \rightarrow \gamma\gamma\pi^0)_{\text{NR}} = (6.16 \pm 0.64 \pm 0.67) \times 10^{-4}$, which agrees with the upper limit measured by the GAMS-2000 experiment [59]. As a validation of the fit, the product branching fraction with the omega intermediate state involved is obtained to be $\mathcal{B}(\eta' \rightarrow \gamma\omega) \cdot \mathcal{B}(\omega \rightarrow \gamma\pi^0) = (2.37 \pm 0.07 \pm 0.18) \times 10^{-3}$, which is consistent with the PDG value [17]. Hopefully this first result will trigger new theory analyses of the

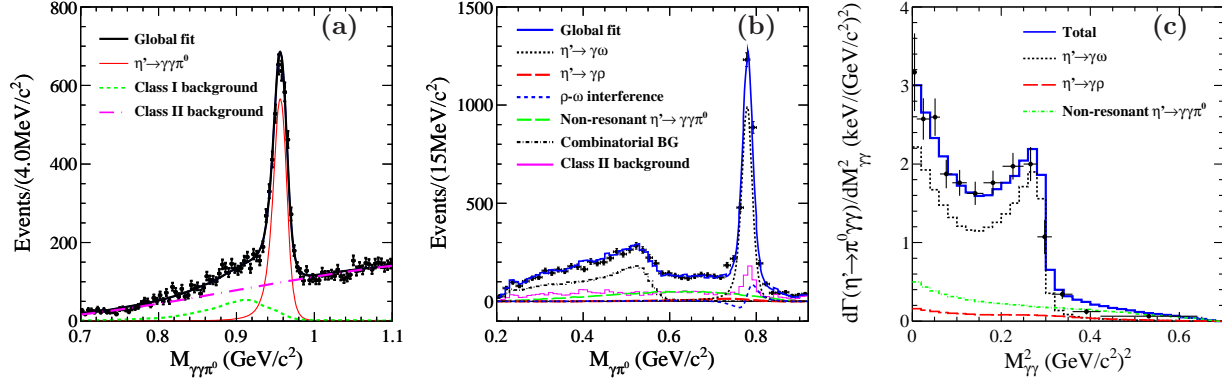


Fig. 15. (a) Distribution of $M(\gamma\gamma\pi^0)$ for the selected inclusive $\eta' \rightarrow \gamma\gamma\pi^0$ signal events. The dotted and dot-dashed curve are the of the background contributions. The total fit result is shown as the solid line. (b) Distribution of $M(\gamma\pi^0)$ and fit result (solid line). The dotted-curve is the ω -contribution; the long dashed-curve ρ^0 -contribution; the short dashed-curve is the ρ^0 - ω interference. The other curves are described in the picture. (c) Acceptance corrected and normalized to the partial width (in keV) $M^2(\gamma\gamma)$ distribution for the inclusive $\eta' \rightarrow \gamma\gamma\pi^0$ decay. The error includes the statistic and systematic uncertainties. The (blue) histogram is the incoherent sum of ρ^0 and ω and the non-resonant components from MC simulations; the (back) dotted-curve is ω -contribution; the (red) dot-dashed-curve is the ρ^0 -contribution; and the (green) dashed-curve is the non-resonant contribution.

decay. In particular a combined analysis of this decay with $\eta' \rightarrow \pi^+\pi^-\pi^0\gamma$ might provide more details about role of isoscalar mesons and isospin violating processes to the η' transition form factor.

4 Rare decays

4.1 Invisible decays [99]

Studies of η , η' decays where one or more products escape detection is a sensitive probe for new light particles beyond the SM. A two-body hadronic decay $J/\psi \rightarrow \phi\eta(\eta')$ is well suited to tag production of η/η' mesons since the presence of undetected particles could be established by missing four-momentum. The ϕ meson is reconstructed efficiently and with good resolution from the K^+K^- decay. The method was first applied for searches of the invisible decays of η/η' (*i.e.* where none of the decay products is observed) at BESII experiment in 2005 [100].

At BESIII the search for the invisible decays of η and η' was repeated using 2009 data set *i.e.* with the statistics of four times larger than BESII. The event selection requires exactly two tracks with opposite charges, identified as kaons. Figure 16(a) shows invariant mass of the kaons, $M(K^+K^-)$, with a clear ϕ peak, while no evident η or η' signal is observed in the mass spectrum for the ϕ recoil system as shown in Fig. 16(b). To reduce the systematic uncertainty, the $\eta(\eta') \rightarrow \gamma\gamma$ decay is also identified in $J/\psi \rightarrow \phi\eta(\eta')$, and the ratios of $\mathcal{B}(\eta(\eta') \rightarrow invisible)$ to $\mathcal{B}(\eta(\eta') \rightarrow \gamma\gamma)$ are determined. Using the world averages [17] for the two photon branching fractions of η and η' , the following 90% C.L. upper limits are obtained $\mathcal{B}(\eta \rightarrow invisible) < 1.32 \times 10^{-4}$ and

$$\mathcal{B}(\eta' \rightarrow invisible) < 5.31 \times 10^{-4}.$$

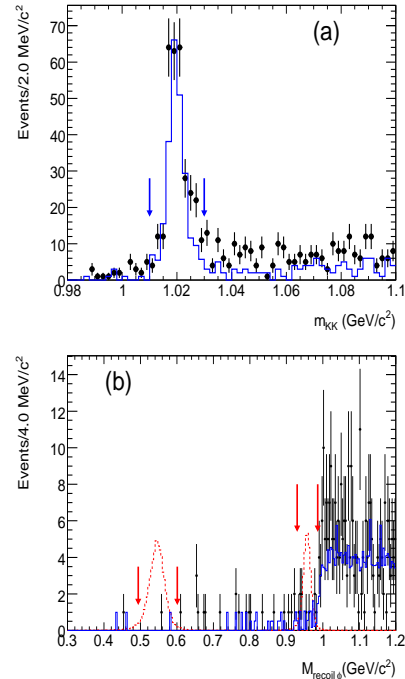


Fig. 16. (a) $M(K^+K^-)$ distribution; (b) Recoil mass distribution against ϕ candidates, M_ϕ^{recoil} , for events with $1.01 \text{ GeV}/c^2 < M(K^+K^-) < 1.03 \text{ GeV}/c^2$ in (a). Points with error bars are data; the (blue) solid histogram is the sum of the expected backgrounds; the dashed histograms (with arbitrary scale) are signals of η and η' invisible decays from MC simulations; the arrows on the plot indicate the signal regions of the η and $\eta' \rightarrow invisible$.

4.2 $\eta/\eta' \rightarrow \pi^+ e^- \bar{\nu}_e + c.c.$ [101]

Within the framework of the chiral perturbation theory, the upper bound of the branching fraction $\eta \rightarrow \pi^+ l^- \bar{\nu}_l$ is predicted to be 2.6×10^{-13} . After considering scalar or vector type interaction, the branching fraction of $\eta \rightarrow \pi^+ l^- \bar{\nu}_l$ was estimated to be $10^{-8} - 10^{-9}$ [102, 103], which is a few orders of magnitudes higher than that in the SM. Therefore, searches for the $\eta \rightarrow \pi^+ l^- \bar{\nu}_l$ and $\eta' \rightarrow \pi^+ l^- \bar{\nu}_l$ at the branching fractions level of $10^{-8} - 10^{-9}$ and below will provide information on the new physics beyond the SM.

At BESIII the searches for the decays of η and $\eta' \rightarrow \pi^+ e^- \bar{\nu}_e + c.c.$ were performed using $J/\psi \rightarrow \phi\eta$ and $\phi\eta'$ with the ϕ meson reconstructed using $K^+ K^-$ decay. No signals are observed in the $\pi^+ e^- \bar{\nu}_e$ mass spectrum shown in Fig. 17 for either η or η' , and upper limits at the 90% C.L. are determined to be 7.3×10^{-4} and 5.0×10^{-4} for the ratios $\mathcal{B}(\eta \rightarrow \pi^+ e^- \bar{\nu}_e + c.c.)/\mathcal{B}(\eta \rightarrow \pi^+ \pi^- \pi^0)$ and $\mathcal{B}(\eta' \rightarrow \pi^+ e^- \bar{\nu}_e + c.c.)/\mathcal{B}(\eta' \rightarrow \pi^+ \pi^- \eta)$, respectively. Using the known values of $\mathcal{B}(\eta \rightarrow \pi^+ \pi^- \pi^0)$ and $\mathcal{B}(\eta' \rightarrow \pi^+ \pi^- \eta)$, the 90% C.L. upper limits for the semileptonic decay rates are $\mathcal{B}(\eta \rightarrow \pi^+ e^- \bar{\nu}_e + c.c.) < 1.7 \times 10^{-4}$ and $\mathcal{B}(\eta' \rightarrow \pi^+ e^- \bar{\nu}_e + c.c.) < 2.2 \times 10^{-4}$.

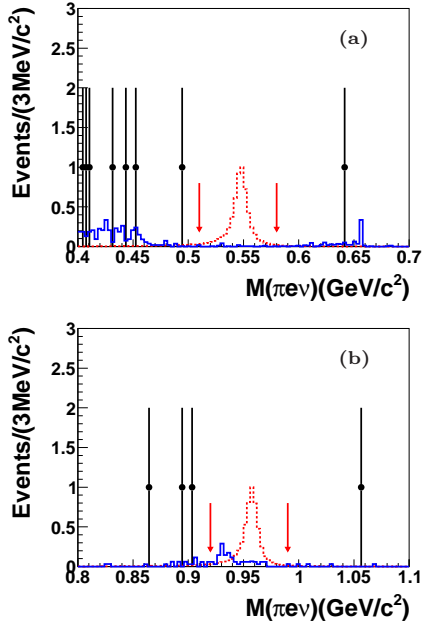


Fig. 17. The $M(\pi^+ e^- \bar{\nu}_e)$ distributions of candidate events: (a) for $J/\psi \rightarrow \phi\eta$ ($\eta \rightarrow \pi^+ e^- \bar{\nu}_e$); (b) for $J/\psi \rightarrow \phi\eta'$ ($\eta' \rightarrow \pi^+ e^- \bar{\nu}_e$). For both (a) and (b): the data (dots with error bars) are compared to the signal MC samples (red dashed histogram) and the expected backgrounds (solid blue histogram). The arrows on the plots indicate the signal regions of η and η' candidates.

4.3 $\eta/\eta' \rightarrow \pi\pi$ [104]

In the SM, these processes can proceed via the weak interaction with a branching fraction of order 10^{-27} according to Ref. [105]. Higher branching fractions are possible either by introducing a CP violating term in the QCD lagrangian (a branching fraction up to 10^{-17} can be obtained in this scheme) or allowing CP violation in the extended Higgs sector (with \mathcal{B} up to 10^{-15}), as described in Ref. [105]. The detection of these decays at any level accessible today would signal P and CP violations from new sources, beyond any considered extension of the SM.

In BESIII analysis of the 2009 data set, the CP and P violating decays of $\eta/\eta' \rightarrow \pi^+ \pi^-$ and $\pi^0 \pi^0$ were searched in J/ψ radiative decays. The mass spectra of $\pi^+ \pi^-$ and $\pi^0 \pi^0$ are shown in Fig. 18 and Fig. 19, respectively. No significant η or η' signal is observed. Using the Bayesian method, the 90% C.L. upper limits are determined to be $\mathcal{B}(\eta \rightarrow \pi^+ \pi^-) < 3.9 \times 10^{-4}$, $\mathcal{B}(\eta' \rightarrow \pi^+ \pi^-) < 5.5 \times 10^{-5}$, $\mathcal{B}(\eta \rightarrow \pi^0 \pi^0) < 6.9 \times 10^{-4}$ and $\mathcal{B}(\eta' \rightarrow \pi^0 \pi^0) < 4.5 \times 10^{-4}$.

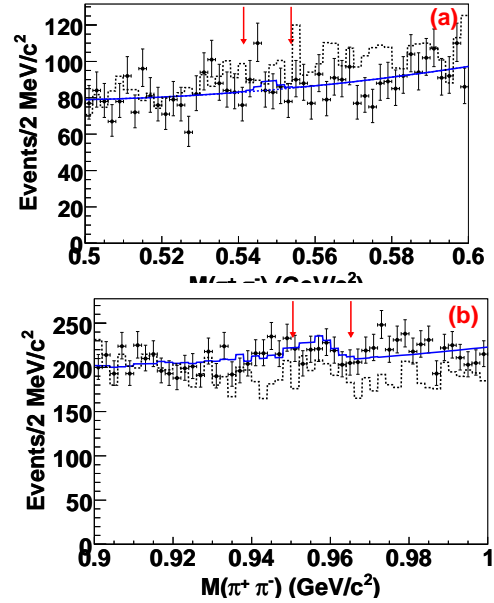


Fig. 18. The $\pi^+ \pi^-$ invariant mass distributions of the final candidate events, (a) η mass region, (b) η' mass regions. The dots with error bars are data, the solid lines are the fit described in the text, and the dashed histograms are the sum of all the simulated normalized backgrounds. The arrows show mass regions which should contain 95% of the signal according to MC simulations.

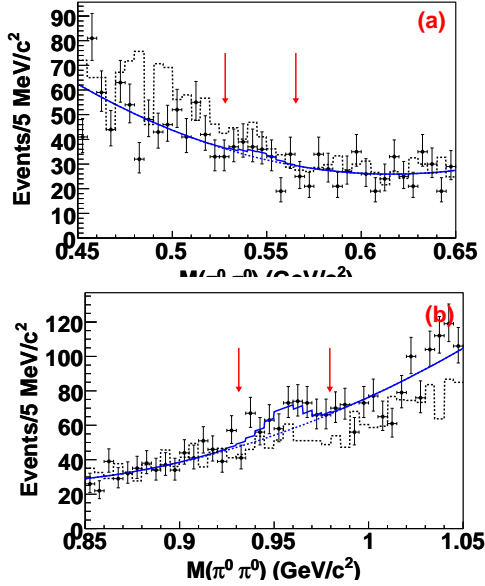


Fig. 19. The $\pi^0\pi^0$ invariant mass distributions of the final candidate events, (a) η mass region, (b) η' mass regions. The dots with error bars are the data, the solid lines are the fit described in the text, and the dashed histograms are the sum of all the simulated normalized backgrounds. The arrows show mass regions which should contain 95% of the signal according to MC simulations.

4.4 $\eta' \rightarrow K^\pm\pi^\mp$ [106]

Non-leptonic weak decays are valuable tools for exploring physics beyond the SM. Among the non-leptonic decays, the decay $\eta' \rightarrow K^\pm\pi^\mp$ is of special interest due to the long-standing problem of the $\Delta I = 1/2$ rule in weak non-leptonic interactions. The branching fraction of $\eta' \rightarrow K^\pm\pi^\mp$ decay is predicted to be of the order of 10^{-10} or higher [107], with a large long-range hadronic contribution expected.

A search for the non-leptonic weak decay $\eta' \rightarrow K^\pm\pi^\mp$ is performed for the first time through the $J/\psi \rightarrow \phi\eta'$ decay, while no evidence for $\eta' \rightarrow K^\pm\pi^\mp$ is seen in the $K\pi$ mass spectrum (Fig. 20). Thus the 90% C.L. upper limit on $\mathcal{B}(\eta' \rightarrow K^\pm\pi^\mp)$ of 3.8×10^{-5} is reported.

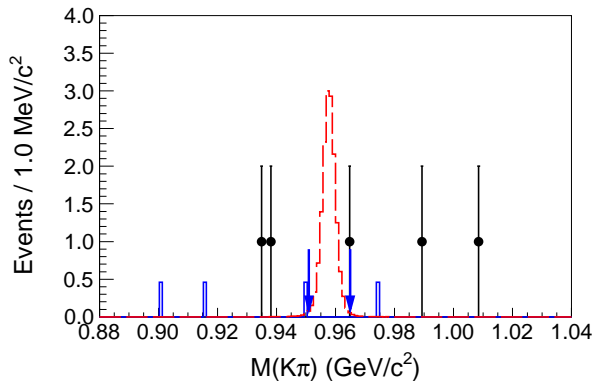


Fig. 20. The $K^\pm\pi^\mp$ invariant mass distribution, where the arrows show the signal region. The dots with error bars are the data, the dashed histogram is for the signal MC with arbitrary normalization, and the solid histogram is the background contamination from a MC simulation of $J/\psi \rightarrow \phi\pi^+\pi^-$.

5 Summary

J/ψ decays provide a clean source of η' for the decay studies. Based on the world largest sample of J/ψ events, the recent results on η/η' decays achieved at the BESIII experiment are presented. In addition to the improved accuracy on the branching fractions of η' , observation of η' new decay modes, including $\eta' \rightarrow \pi^+\pi^-\pi^+\pi^-$, $\eta' \rightarrow \pi^+\pi^-\pi^0\pi^0$, $\eta' \rightarrow \rho^\mp\pi^\pm$ and $\eta' \rightarrow \gamma e^+e^-$, were reported for the first time. Precision of $\eta' \rightarrow \pi^+\pi^-\gamma$ $M(\pi^+\pi^-)$ distribution from BESIII with clear $\rho^0-\omega$ interference is comparable to the $e^+e^- \rightarrow \pi^+\pi^-$ data and allows to compare these two reactions in both model dependent and model independent way. In particular a competitive extraction of $\omega \rightarrow \pi^+\pi^-$ branching fraction is possible. It is found that an extra contribution is necessary to describe data besides the contributions from $\rho^0(770)$ and ω .

Despite the impressive progress, many η/η' decays are still to be observed and explored. The BESIII detector will collect a sample of 10^{10} J/ψ events in the near future, which offers great prospects for research in η/η' physics with unprecedented precision.

A list of the specific decay channels where important impact of the new data is expected includes:

- Larger data samples of $\eta \rightarrow \pi^+\pi^-\pi^0$ and $\eta \rightarrow \pi^0\pi^0\pi^0$ decays from BESIII experiment are needed to provide independent check of the analyses carried out at other experiments. The Dalitz plot distributions will be made available for the direct fits to theory. In particular data from the planned run will allow to collect approximately 0.5×10^6 events of $\eta \rightarrow \pi^+\pi^-\pi^0$ with negligible background. In addition one could probably also use other J/ψ decay modes as sources of η mesons. Some possible examples are $J/\psi \rightarrow \omega\eta$ ($\mathcal{B} = (1.74 \pm 0.20) \times 10^{-3}$) and $J/\psi \rightarrow p\bar{p}\eta$ ($\mathcal{B} = (2.00 \pm 0.12) \times 10^{-3}$).
- For $\eta' \rightarrow \pi^+\pi^-\eta$ and $\eta' \rightarrow \pi^0\pi^0\eta$ decays the analysis could be extended not only by using the new data but also by reconstructing the final states with three pion decay modes of η in addition to $\eta \rightarrow \gamma\gamma$. The increased statistics would allow *e.g.* to search for the cusp in $\eta' \rightarrow \pi^0\pi^0\eta$ and provide further information about $\eta\pi$ scattering [57]. In addition the use of the same final state topology $\eta' \rightarrow \pi^+\pi^-(\eta \rightarrow$

$\pi^0\pi^0\pi^0$) and $\eta' \rightarrow \pi^0\pi^0(\eta \rightarrow \pi^+\pi^-\pi^0)$ will enable to determine ratio of the two decay modes with low systematic uncertainty.

- For $\eta' \rightarrow \pi^0\pi^0\pi^0$ and $\eta' \rightarrow \pi^+\pi^-\pi^0$ larger statistics is crucial to carry out amplitude analysis of the processes. At present it is impossible to differentiate between S and D waves. A detailed understanding of this process dynamics is a prerequisite for a program of light quark masses determination from comparison to the $\eta' \rightarrow \pi\pi\eta$ processes, a method which do not rely on the full decay width value. Several theory groups has expressed interest in description of the decay within dispersive approach. The overall goal is understanding of all parity even processes of η and η' .
- Hadronic parity odd processes $\eta' \rightarrow \pi^+\pi^-\pi^+\pi^-$, $\pi^+\pi^-\pi^0\pi^0$ offers a window to study double off shell transition form factor of η' . The ultimate goal would be to carry out amplitude analysis of the reactions. The new data with expected about 1200 events would allow for a first stage of such analysis. However, the collected data on these decays together with $\eta' \rightarrow \pi^+\pi^-e^+e^-$ decay will already provide unique constraints and checks for the models of the η' double off shell transition form factor. In addition, since the predicted branching fraction for the related $\eta' \rightarrow \pi^+\pi^-\mu^+\mu^-$ process is about 2×10^{-5} , the decay likely will be observed with the new data. The branching fraction value of this decay is sensitive to the η' transition form factor.
- For $\eta' \rightarrow \pi^+\pi^-e^+e^-$ decay much progress is expected. A combined analysis of 2012 and the new run data will allow for a sample close to 2×10^4 events. In particular a CP symmetry test by measurement of asymmetry between the lepton and the pion decay planes [108, 109] as well as studies of the $M(e^+e^-)$ and $M(\pi^+\pi^-)$ distributions would be possible.
- Among the discussed in this review very rare decays of η/η' the largest impact of the new data is expected for invisible decays, $\eta/\eta' \rightarrow \pi^+e^-\bar{\nu}_e$ and $\eta' \rightarrow K^\pm\pi^\mp$ where no background was observed. Therefore the sensitivity should scale with luminosity. In addition the results for the first two decay modes are based on the 2009 data set only.

Both η and η' decays are important tools for studies of strong interactions in non-perturbative region and for determination of some SM parameters. In addition they provide an indirect way to probe physics beyond the standard model. In particular the pursued at BES-III η and η' decay program, where the data collected

at J/ψ are used for wealth of other studies, represents smart and resource efficient research strategy.

References

- 1 A. Pevsner *et al.*, Phys. Rev. Lett. **7**, 421 (1961).
- 2 G. R. Kalbfleisch *et al.*, Phys. Rev. Lett. **12**, 527 (1964).
- 3 M. Goldberg *et al.*, Phys. Rev. Lett. **12**, 546 (1964).
- 4 J. Gasser and H. Leutwyler, Annals Phys. **158**, 142 (1984).
- 5 J. Wess and B. Zumino, Phys. Lett. **37B**, 95 (1971).
- 6 E. Witten, Nucl. Phys. **B223**, 422 (1983).
- 7 J. Bijnens, A. Bramon and F. Cornet, Z. Phys. **C46**, 599 (1990).
- 8 J. J. Sakurai, Annals Phys. **11**, 1 (1960).
- 9 L. G. Landsberg, Phys. Rept. **128**, 301 (1985).
- 10 R. Kaiser and H. Leutwyler, Eur. Phys. J. **C17**, 623 (2000).
- 11 M. Ablikim *et al.* (BESIII), Phys. Rev. Lett. **118**, 012001 (2017).
- 12 M. Ablikim *et al.* (BESIII), Phys. Rev. **D92**, 012001 (2015).
- 13 M. Ablikim *et al.* (BESIII), Phys. Rev. **D92**, 051101 (2015).
- 14 M. Ablikim *et al.* (BESIII), Phys. Rev. **D96**, 012005 (2017).
- 15 M. Ablikim *et al.* (BESIII), Phys. Rev. Lett. **112**, 251801 (2014), [Addendum: Phys. Rev. Lett.113,039903(2014)].
- 16 M. Ablikim *et al.* (BESIII), Nucl. Instrum. Meth. **A614**, 345 (2010).
- 17 C. Patrignani *et al.* (Particle Data Group), Chin. Phys. **C40**, 100001 (2016).
- 18 M. Ablikim *et al.* (BESIII), Chin. Phys. **C36**, 915 (2012).
- 19 M. Ablikim *et al.* (BESIII), Chin. Phys. **C41**, 013001 (2017).
- 20 M. Ablikim *et al.* (BESIII), Phys. Rev. **D92**, 012014 (2015).
- 21 D. G. Sutherland, Phys. Lett. **23**, 384 (1966).
- 22 J. S. Bell and D. G. Sutherland, Nucl. Phys. **B4**, 315 (1968).
- 23 R. Baur, J. Kambor and D. Wyler, Nucl. Phys. **B460**, 127 (1996).
- 24 C. Ditsche, B. Kubis and U.-G. Meissner, Eur. Phys. J. **C60**, 83 (2009).
- 25 H. Leutwyler, Phys. Lett. **B378**, 313 (1996).
- 26 H. Osborn and D. J. Wallace, Nucl. Phys. **B20**, 23 (1970).
- 27 J. Gasser and H. Leutwyler, Nucl. Phys. **B250**, 539 (1985).
- 28 J. Kambor, C. Wiesendanger and D. Wyler, Nucl. Phys. **B465**, 215 (1996).
- 29 A. V. Anisovich and H. Leutwyler, Phys. Lett. **B375**, 335 (1996).
- 30 J. Bijnens and K. Ghorbani, JHEP **11**, 030 (2007).
- 31 S. P. Schneider, B. Kubis and C. Ditsche, JHEP **02**, 028 (2011).
- 32 K. Kampf, M. Knecht, J. Novotny and M. Zdrahal, Phys. Rev. **D84**, 114015 (2011).
- 33 G. Colangelo, S. Lanz, H. Leutwyler and E. Passemar, PoS **EPS-HEP2011**, 304 (2011).
- 34 G. Colangelo, S. Lanz, H. Leutwyler and E. Passemar, Phys. Rev. Lett. **118**, 022001 (2017).
- 35 P. Guo *et al.*, Phys. Rev. **D92**, 054016 (2015).
- 36 F. Ambrosino *et al.* (KLOE), JHEP **05**, 006 (2008).
- 37 J. Bijnens and J. Gasser, Phys. Scripta **T99**, 34 (2002).
- 38 B. Borasoy and R. Nissler, Eur. Phys. J. **A26**, 383 (2005).
- 39 J. G. Layter *et al.*, Phys. Rev. **D7**, 2565 (1973).
- 40 A. Abele *et al.* (Crystal Barrel), Phys. Lett. **B417**, 197 (1998).
- 41 P. Adlarson *et al.* (WASA-at-COSY), Phys. Rev. **C90**, 045207 (2014).
- 42 A. Anastasi *et al.* (KLOE-2), JHEP **05**, 019 (2016).
- 43 C. O. Gullstrom, A. Kupsc and A. Rusetsky, Phys. Rev. **C79**, 028201 (2009).
- 44 F. Ambrosino *et al.* (KLOE), Phys. Lett. **B694**, 16 (2011).
- 45 C. Adolph *et al.* (WASA-at-COSY), Phys. Lett. **B677**, 24 (2009).
- 46 S. Prakhov *et al.* (Crystal Ball at MAMI, A2), Phys. Rev. **C79**, 035204 (2009).
- 47 M. N. Achasov *et al.*, JETP Lett. **73**, 451 (2001), [Pisma

- Zh. Eksp. Teor. Fiz.73,511(2001)].
- 48 A. Abele *et al.* (Crystal Barrel), Phys. Lett. **B417**, 193 (1998).
- 49 D. Alde *et al.* (Serpukhov-Brussels-Annecy(LAPP), Soviet-CERN), Z. Phys. **C25**, 225 (1984), [Yad. Fiz.40,1447(1984)].
- 50 M. Ablikim *et al.* (BESIII), Phys. Rev. **D83**, 012003 (2011).
- 51 M. Ablikim *et al.* (BESIII), arXiv:1709.04627.
- 52 R. Escribano, P. Masjuan and J. J. Sanz-Cillero, JHEP **05**, 094 (2011).
- 53 V. Dorofeev *et al.*, Phys. Lett. **B651**, 22 (2007).
- 54 A. M. Blik *et al.*, Phys. Atom. Nucl. **71**, 2124 (2008), [Yad. Fiz.71,2161(2008)].
- 55 P. Adlarson *et al.*, arXiv:1708.04230.
- 56 B. Kubis and S. P. Schneider, Eur. Phys. J. **C62**, 511 (2009).
- 57 T. Isken, B. Kubis, S. P. Schneider and P. Stoffer, Eur. Phys. J. **C77**, 489 (2017).
- 58 F. G. Binon *et al.* (Serpukhov-Brussels-Annecy(LAPP)), Phys. Lett. **140B**, 264 (1984).
- 59 D. Alde *et al.* (Serpukhov-Brussels-Los Alamos-Annecy(LAPP)), Z. Phys. **C36**, 603 (1987).
- 60 M. Ablikim *et al.* (BESIII), Phys. Rev. Lett. **108**, 182001 (2012).
- 61 D. J. Gross, S. B. Treiman and F. Wilczek, Phys. Rev. **D19**, 2188 (1979).
- 62 B. Borasoy, U.-G. Meissner and R. Nissler, Phys. Lett. **B643**, 41 (2006).
- 63 P. Naik *et al.* (CLEO), Phys. Rev. Lett. **102**, 061801 (2009).
- 64 F.-K. Guo, B. Kubis and A. Wirzba, Phys. Rev. **D85**, 014014 (2012).
- 65 D. Parashar, Phys. Rev. **D19**, 268 (1979).
- 66 M. Gell-Mann, D. Sharp and W. G. Wagner, Phys. Rev. Lett. **8**, 261 (1962).
- 67 W. Bartel *et al.* (JADE), Phys. Lett. **113B**, 190 (1982).
- 68 H. J. Behrend *et al.* (CELLO), Phys. Lett. **114B**, 378 (1982), [Erratum: Phys. Lett.125B,518(1983)].
- 69 C. Berger *et al.* (PLUTO), Phys. Lett. **142B**, 125 (1984).
- 70 M. Althoff *et al.* (TASSO), Phys. Lett. **147B**, 487 (1984).
- 71 H. Aihara *et al.* (TPC/Two Gamma), Phys. Rev. **D35**, 2650 (1987).
- 72 H. Albrecht *et al.* (ARGUS), Phys. Lett. **B199**, 457 (1987).
- 73 S. I. Bityukov *et al.*, Z. Phys. **C50**, 451 (1991).
- 74 M. Benayoun *et al.*, Z. Phys. **C58**, 31 (1993).
- 75 A. Abele *et al.* (Crystal Barrel), Phys. Lett. **B402**, 195 (1997).
- 76 M. Acciarri *et al.* (L3), Phys. Lett. **B418**, 399 (1998).
- 77 F. Stollenwerk, C. Hanhart, A. Kupsc, U. G. Meissner and A. Wirzba, Phys. Lett. **B707**, 184 (2012).
- 78 P. Adlarson *et al.* (WASA-at-COSY), Phys. Lett. **B707**, 243 (2012).
- 79 D. Babusci *et al.* (KLOE), Phys. Lett. **B718**, 910 (2013).
- 80 C. Hanhart, A. Kupsc, U. G. Meißner, F. Stollenwerk and A. Wirzba, Eur. Phys. J. **C73**, 2668 (2013), [Erratum: Eur. Phys. J.C75, 242(2015)].
- 81 G. J. Gounaris and J. J. Sakurai, Phys. Rev. Lett. **21**, 244 (1968).
- 82 R. Garcia-Martin, R. Kaminski, J. R. Pelaez, J. Ruiz de Elvira and F. J. Yndurain, Phys. Rev. **D83**, 074004 (2011).
- 83 B. Kubis and J. Plenter, Eur. Phys. J. **C75**, 283 (2015).
- 84 M. Ablikim *et al.* (BESIII), Phys. Rev. **D87**, 092011 (2013).
- 85 A. Faessler, C. Fuchs and M. I. Krivoruchenko, Phys. Rev. **C61**, 035206 (2000).
- 86 B. Borasoy and R. Nissler, Eur. Phys. J. **A33**, 95 (2007).
- 87 T. Petri, Anomalous decays of pseudoscalar mesons, Master's thesis Julich, Forschungszentrum 2010
arXiv:1010.2378 [nucl-th].
- 88 MesonNet Workshop on Meson Transition Form Factors 2012 arXiv:1207.6556 [hep-ph].
- 89 T. Blum *et al.* (2013), arXiv:1311.2198 [hep-ph].
- 90 V. M. Budnev and V. A. Karnakov, Pisma Zh. Eksp. Teor. Fiz. **29**, 439 (1979).
- 91 R. I. Dzhelyadin *et al.*, Phys. Lett. **88B**, 379 (1979), [JETP Lett.30,359(1979)].
- 92 A. Bramon and E. Masso, Phys. Lett. **B104**, 311 (1981).
- 93 L. Ametller, L. Bergstrom, A. Bramon and E. Masso, Nucl. Phys. **B228**, 301 (1983).
- 94 L. Ametller, J. Bijmens, A. Bramon and F. Cornet, Phys. Rev. **D45**, 986 (1992).
- 95 H. J. Behrend *et al.* (CELLO), Z. Phys. **C49**, 401 (1991).
- 96 C. Terschlüsen, S. Leupold and M. F. M. Lutz, Eur. Phys. J. **A48**, 190 (2012).
- 97 R. Jora, Nucl. Phys. Proc. Suppl. **207-208**, 224 (2010).
- 98 R. Escribano, PoS **QNP2012**, 079 (2012).
- 99 M. Ablikim *et al.* (BESIII), Phys. Rev. **D87**, 012009 (2013).
- 100 M. Ablikim *et al.* (BES), Phys. Rev. Lett. **97**, 202002 (2006).
- 101 M. Ablikim *et al.* (BESIII), Phys. Rev. **D87**, 032006 (2013).
- 102 P. Fayet, Phys. Rev. **D74**, 054034 (2006).
- 103 P. Fayet, Phys. Rev. **D75**, 115017 (2007).
- 104 M. Ablikim *et al.* (BESIII), Phys. Rev. **D84**, 032006 (2011).
- 105 C. Jarlskog and E. Shabalin, Phys. Scripta **T99**, 23 (2002).
- 106 M. Ablikim *et al.* (BESIII), Phys. Rev. **D93**, 072008 (2016).
- 107 L. Bergstrom and H. R. Rubinstein, Phys. Lett. **B203**, 183 (1988).
- 108 C. Q. Geng, J. N. Ng and T. H. Wu, Mod. Phys. Lett. **A17**, 1489 (2002).
- 109 D. N. Gao, Mod. Phys. Lett. **A17**, 1583 (2002).